AIAA

MISSILE SCIENCES CONFERENCE

MONTEREY, CALIFORNIA

29 NOVEMBER - 1 DECEMBER 1988

VOLUME 6

NAVY BALLISTIC MISSILE TECHNOLOGY

PAPERS PRESENTED AT SESSION 6

WEDNESDAY (P.M.) 30 NOVEMBER 1988

AIAA

MISSILE SCIENCES CONFERENCE

MONTEREY, CALIFORNIA

29 NOVEMBER - 1 DECEMBER 1988

VOLUME 6

NAVY BALLISTIC MISSILE TECHNOLOGY

PAPERS PRESENTED AT SESSION 6

WEDNESDAY (P.M.) 30 NOVEMBER 1988

Chairman: CAPT John T. Mitchell (USN), SSP

Vice Chairman: Robert Ginn, LMSC

Three papers were submitted for inclusion in Volume 6. All pesentation titles and the authors are listed below, along with their phone numbers. A check in the margin denotes that a paper is included in this volume.

DEFENSE RESPONSIVE FAST BURN MISSILE SYSTEMS

Thomas O. Morgan
Lawrence Livermore National Laboratory
D Division - P. O. Box 808 L-86
Livermore, CA 94550
Phone: (415) 422-8819

NEW MATERIALS FOR STRATEGIC SYSTEMS HARDENING AGAINST HIGH IRRADIANCE LASER THREATS

Bernard Laub and John Rhodehamel
Acurex Corporation
520 Clyde Avenue - P. O. Box 7040
Mountain View, CA 94039
Phone: (415) 961-6100

LASER HARDENING AND COUNTERMEASURES CONCEPTS FOR ADVANCED BALLISTIC MISSILES

W. F. Bozich and O. K. Salmassy
McDonnell Douglas Astronautics Company
5301 Bolsa Avenue
Huntington Beach, CA 92647
Phone: (714) 896-1341

✓ DATA ANALYSIS FOR PLUME MEASUREMENTS

Charles Allen
RDA
P. O. Box 9377
Albuquerque, NM 87119
Phone: (505) 844-0434

Dr. Arthur Lane
JPL - Space Sciences Div. - MS 183501
4800 Oak Grove Drive
Pasadena, CA 91109
Phone: (818) 354-2725

AVIONICS FOR A FRACTIONATED SLBM

Robert E. Brainard
Lockheed Missiles & Space Co., Inc.
Advanced Concepts, 0/81-71, Bldg. 157
Sunnyvale, CA 94088-3504
Phone: (408) 756-3122

A RING LASER GYRO BASED STELLAR AIDED INERTIAL NAVIGATION SYSTEM

Shing Peter Kau
Honeywell Space and Strategic Avionics Div.
MS FL51-887-3
13350 U. S. Highway 19, South
Clearwater, FL 34624

A METHODOLOGY AND CAE TOOL SET FOR RADIATION HARDENED VLSI APPLICATION SPECIFIC INTEGRATED CIRCUIT DESIGN

Greg Kuchta
Lockheed Missiles & Space Co., Inc.
Electronics Guidance/Flight Controls
0/81-61, Bldg. 157
Sunnyvale, CA 94088-3504
Phone (408) 756-0175

SOME NEW GUIDANCE CONCEPTS

Bud Bergman
General Electric Company - RESD
3198 Chestnut Street - Room 6419
Philadelphia, PA 19101
Phone: (215) 823-2374

ULTRAVIOLET AND VISIBLE PLUME MEASUREMENTS OF NOVEMBER 1987 (U)

Mr. Charles Allen*
R & D Associates

Dr. Arthur Lane
Mr. Bradford D. Wallis
Jet Propulsion Laboratory

Abstract

This experiment collected and reported on visible and ultraviolet signatures from the second stage of a solid propellant missile ladened with aluminum oxide particulate. The analyses focused on absolute ultraviolet (UV) radiometrics of the booster plume and its afterburn as a function of altitude. (Afterburn is the reignition of fuel rich missile exhaust with the atmospheric oxidizers.) The stability of the booster plume as a pointing and tracking source for hardbody handoff was also to be examined. The plumes were relatively large and bright (some data were saturated), although the UV was about 1/2 the size of the visible. Furthermore, anomalous events such as chuffing and quickly varying plume length in the visible were much reduced in the UV. Afterburning outside the ozone region did not appear in the UV. The rapid quenching of the UV light caused by rapid cooling of particulates and entry into the rarified upper regions of the atmosphere leads to the conclusion that automated UV tracking during upper stage thrusting may be more stable than similar tracking in the visible. However for this test, manual track was necessary resulting in high jitter. The consequences of this type of plume are that a centroid tracker that works well with a round target would be hard pressed to find the centroid position along the plume unless it is tracking the UV plume outside the atmosphere. Thus, other trackers or imagers should be considered if one were to track the plume and handoff to the missile in the atmosphere with high resolution optics.

BACKGROUND

There is a limited UV data base on plumes for acquisition, pointing, tracking, and hardbody hand-off on liquid and solid missile launches. In September 1987, an ultraviolet and visible observation of the scheduled test for November 1987 was organized to view a solid propellent missile. Through short-term Herculean efforts of the team from Jet Propulsion Laboratory, LORAL Electro-Optical Division, and Aeromet (the operator of the Learjet optical observatory), an ultraviolet 5.5" telescope and camera was installed in the Learjet. A successful ultraviolet and visible imaging of data collection was accomplished.

SYSTEM DESCRIPTION

The Aeromet High Altitude Learjet Observatory (HALO) is specifically configured for optical observations. The aircraft contains two independent sensor systems, each of which contains a narrow and wide field of view camera, a telescope, and a gimballed pointing mirror. The inertially stabilized gimballed mirror is used to control the line of sight of the sensors. It can be commanded either manually or from an airborne computer. The computer, in turn, uses inputs from an on-board inertial sensor system and either a pre-loaded ephemeris program or telemetry information received from the test range radars to point the sensor line of sight to a target. Both optical systems look out through windows on the right side of the aircraft. The two platforms field of regard overlap by 10° in azimuth.

For the tests described here, an intensified imaging UV camera was used as the narrow field of view sensor for the forward platform, and the other sensors used intensified visible CID focal plane arrays. The two sensor platform gimballed mirrors were manually controlled for these tests by separate operators, resulting in slightly different acquisition times and pointing performance.

The wide field of view acquisition camera for each system has a 3.78 x 5.03 degree field of view. The field of view of the visible data camera was .766° horizontal x .573° vertical. The ultraviolet camera had a field of view of 1.45° horizontal x .9164° vertical. The optical layout for the UV camera is as shown in Figure 1. A similar layout replacing the UV telescope and camera with a 3-1/2-inch visible telescope and camera was used on the rear platform for the visible observation. For both cameras to observe objects, the pilot had to position the aircraft so that the objects were 90°± 5° to the roll axis of the aircraft.

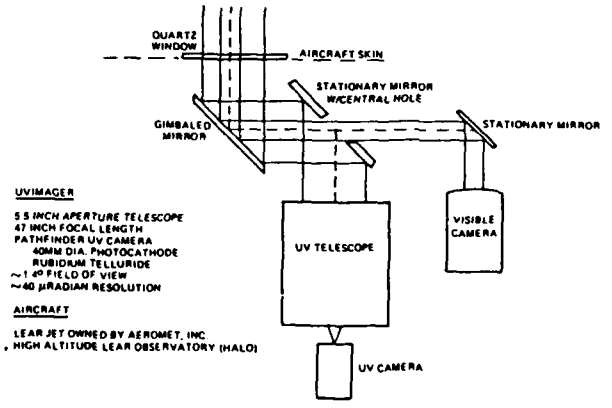

Figure 1. Optical Layout

* Member of AIAA

Data recorded included the four imagers (two tracking cameras, one visible, and one ultraviolet narrow field of view camera) on Sony 5600 recorders, pointing vectors from the inertial navigation system for each tracking camera, IRIG timing and voice. Prior and post mission, the UV camera was calibrated. The visible camera had its field of view and optical path defined. The video recorders were calibrated post mission.

OPERATIONS

To maintain safety and to calculate, after the fact, the line of sight distance from aircraft to object, beacons were installed on both the aircraft and missile. The aircraft and missile were then radar tracked. The missile is a two stage solid propellant system. The propellant constituents in the burning chamber and expanded to 1 psi are given in Table 1.

	(mole/100 grams) In Chamber	(16% Aluminum Loading) Exhausted
Pressure	400 psia	1 psia
Temperature	5046°F	1844°F
H_2	1.407	1.512
Al_2O_3 (solid)	0.283	0.297
CO	1.116	1.059
N_2	0.293	0.294
NCl	0.526	0.579
CO_2	0.032	0.088
H_2O	0.297	0.021
Cl	0.021	trace
$AlCl_2$	0.005	trace
HO	0.006	trace
AlCl	0.016	trace
H	0.084	trace

Table 1. Constituents of Motor Exhaust Gas for the Second Stage of the Observed Missile

Night Mission

On 10 November, the HALO was able to observe the missile launched at 17:49 local time. This was approximately 45 minutes after sundown, making the solar tangent ray at 150 kilometers. Figure 2 shows the geometry. The missile stage burned from 34.5 to 42.8 kilometers altitude causing the camera system to look up 45 to 55°. Separation and thrust neutralization (three plugs on the top of the stage releasing to allow venting through them) followed by a destruct sequence which blew the case (called case venting) occurred immediately after burnout.

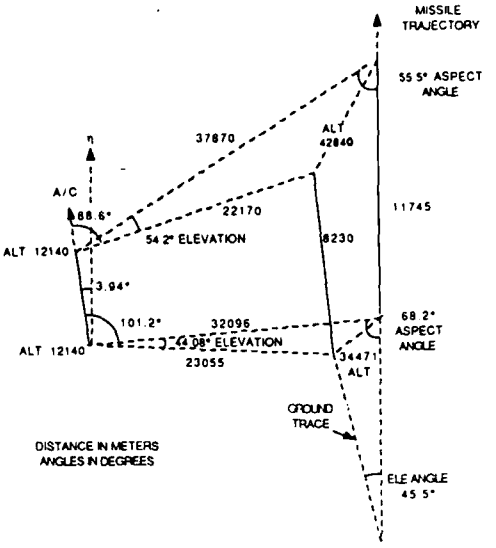

Figure 2. Night Mission Geometry

Visible camera acquisition occurred after first stage burnout by tracking on the hot spent first stage motor which did not separate until second stage ignition. Ultraviolet camera acquisition occurred about halfway through second stage burn and observed from 37 Km to beyond 43 Km altitude including second stage destruction. As explained later, both the visible and ultraviolet cameras saturated giving limited radiometric data.

Day Mission

On 25 November (a clear day) at about 1200 noon, the experiment was repeated. The engagement geometry nearly matched that of the night experiment. The geometry is shown in Figure 3. At launch time, the sun was about 48 degrees from the local Zenith. The ultraviolet camera operator acquired and tracked the first stage motor nozzle through second stage ignition and burnout. A lower gain setting was initially was used to limit and not saturate the ultraviolet camera. As with the night mission, automatic gain control limited the visible camera input, but did not record its settings so that the camera did not yield radiometric data.

The visible camera operator acquired just after second stage destruction, and did not collect meaningful data. The track operators were forced to scan the sky through a limited window to acquire and were fortunate to obtain any data.

DATA REDUCTION

Approach

Since the data were of varied quality, several approaches were taken to maximize the technical gain. The manual tracking resulted in residual line of sight wander and aircraft disturbances caused line of sight jitter. Plume jitter values using centroid and edge tracking algorithms were estimated. The ultraviolet camera was radiometrically calibrated, but the visible data were

recorded through two unrecorded automatic gain controls (one on the ICID and one on the tape recorder) so no quantitative visible radiometry is available. Further, much of the data were saturated. To the extent that the plume is seen in the field of view and the radar beacon data is accurate, a plume size is roughly calculable for the somewhat arbitrary video levels in the visible and UV bands.

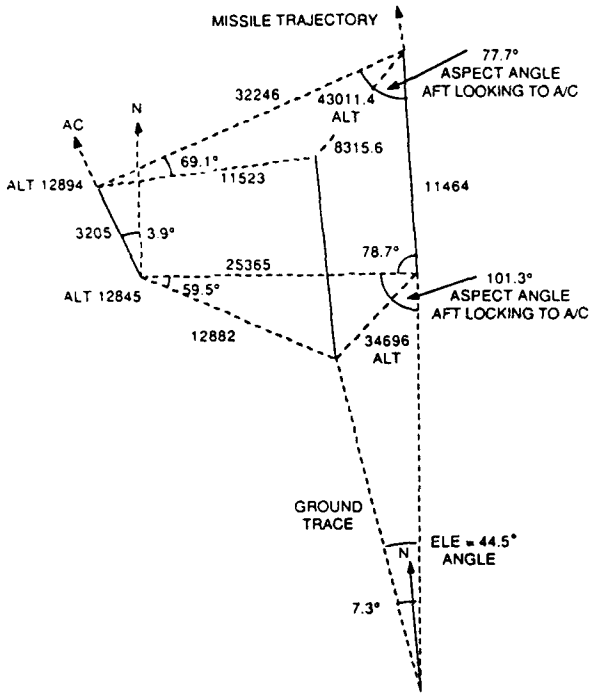

Figure 3. Day Mission Geometry

Ultraviolet Sensor Calibration and Data Extraction Discussion

The short interval between experiment definition and data collection using new equipment resulted in an abbreviated calibration process. Figure 4 provides the total camera efficiency from the quartz transmission cutoff at the short wavelength end, to the region on the red end where one can no longer measure any response using a monochromatic beam into the camera. The line weight in this plot is indicative of the measurement certainty, with the heaviest line representing the lowest measurement errors and least uncertainty. Calibration from 2000 to 3200 angstroms was against two NBS standards. Calibration from 3600 to 4000 angstroms was referenced against a "third party" silicon dioide proported to be traceable to an NBS standard. The data are extrapolated above 4000 angstroms.

The data represent the convolution of the photocathode quantum efficiency, the microchannel plate performance at highest gain (similar to that used in the night mission, the electron bombardment-phosphor activation process, the efficiency of the coupling fiber optic bundles and the CCD efficiency. Because the optical gain of the phosphor system is so high and well coupled into the CCD wavelength response function, it appears that the system efficiency is higher than unity. In reality, the data numbers (DN's) out of the camera as determined by the image analysis system are greater than unity for a single photoelectron event initiated at the photocathode. A single photoelectron event can produce at the highest gain setting, an optical pulse at the CCD which covers more than a 2 x 2 pixel array, at 200+ DN for each pixel. The best estimate at this time, is the peak system performance is about 600% at 254 nm. Thus, the optical gain is estimated to be a factor of 100 when the HALO camera intensified stage is set to 10 volts. This is the normalization factor for the reduction that follows in the subsequent sections.

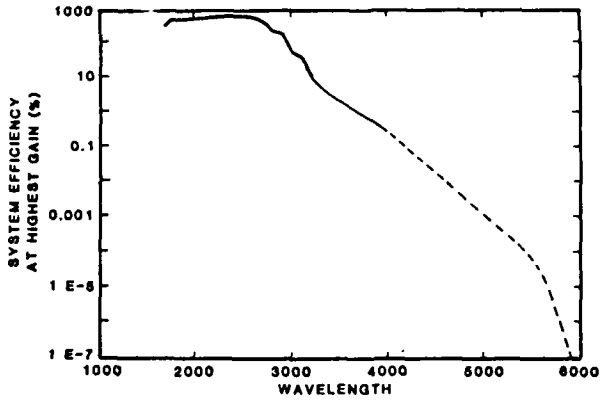

Figure 4. JPL UV Camera System Efficiency

The path of photons from the source object to the recorded tape is shown pictorially in Figure 5. System efficiency was estimated by examining the individual component performance. For elements not directly measured, the best estimate of the upper and lower bounds of performance and the most probable value are provided. The Ferrante mirrors and quartz window were not extracted and calibrated separately. End-to-end calibration was done using stars as sources.

The loss of signal on recording and repeated subsequent playbacks was checked. The worst effect seems to be in the initial recording. Tests showed that for a well maintained Sony 5600, about 10% of the signal strength was lost between the initial record and first playback. If one repeated this test with freshly cleaned tape heads, then the losses were about 6% for the first cycle. After that initial loss, the losses after 10 playbacks were on the order of 1%.

Several Lowtran 6 code runs (with UV atmospheric elements added) were performed to evaluate the transmission coefficients for the atmosphere between the airplane and the missile and for the transmission of solar radiation through the atmosphere to the altitude of the missile. These runs used the correct average altitudes and slant ranges. There is always uncertainty with respect to actual aerosol density scattering centers and hence, estimates can be off significantly if incorrect assumptions are included. No

meteorological data pertinent to UV ozone or aerosols seem to be available for these data sets, so high altitude aerosol extinction is not included in the transmission estimates. This allows other analysts to use their favorite models. Figure 6 is a plot of the attenuation for solar radiation reaching the missile when the measurement time is near local noon and the sun is 48 degrees from the local Zenith. This condition was approximately correct for the day and night missions and without solar radiation.

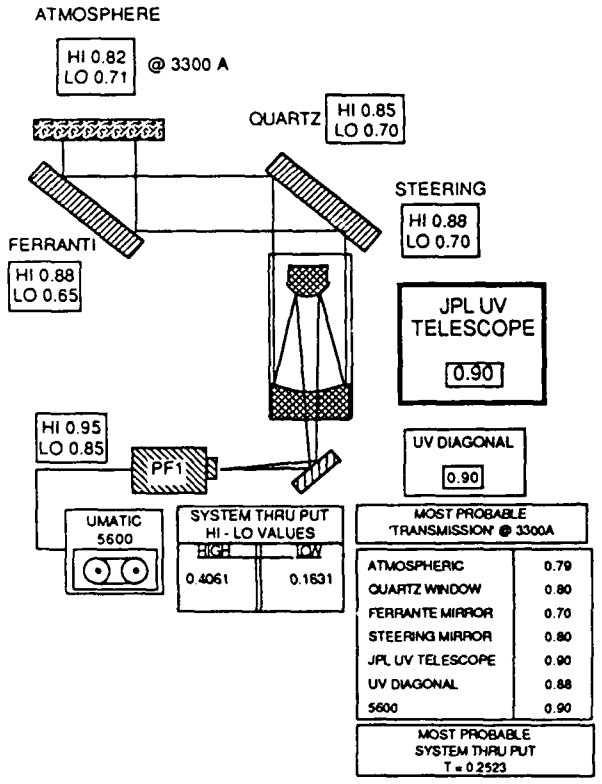

Figure 5. HALO Optical System

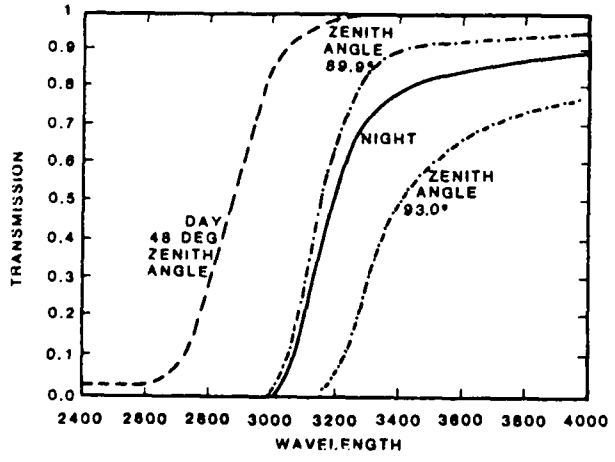

Figure 6. Atmospheric Transmission to 40Km Day Night and Setting Sun

Plume Phenomology Discussion

The unjittered resolution for the day mission was slightly better than the night given the slightly shorter range to the target. For the visible camera, it is .7-.9 meters per pixel and for the ultraviolet camera, it is 1.1 - 1.5 meters. Line of sight movement with respect to the target, causes different effects on the image. Motion that occurs on a time scale of less than the exposure time of a single field will cause smearing of the image. The image distortion normally associated with a raster scanned sensor is generally absent from these sensors because the entire frame is exposed at once and then rastered out from a stored image. Image motion that occurs between the interlaced fields of a frame will cause alternate lines to be offset from each other by an amount corresponding to the average motion between the field exposures. Thus, the resolution of the camera system is poorer than the optical limits just given and probably is on the order of a few meters.

Ultraviolet Data Sets

Night Second Stage Data

The night flight occurred in the late afternoon, local time, when the ground was in the evening twilight shadow and the 40 km altitude region was in the transition zone between penumbra and tangent ray sun light. For such a geometry, the transmission of solar UV light is quite poor, for most of the sun's rays must penetrate many optical depths of atmosphere before reaching the region of the missile. Several Lowtran 6 computations were performed to examine the amount of solar UV energy reaching the altitude of the missile. Our best estimate is that the sun was about 11 degrees below the horizon at the launch site, and that shadow line was at about 150 km altitude, above most of the atmosphere. One would expect little direct solar UV radiation some 100 km further from the shadow line. Three cases with Lowtran 6 were computed to show the transmission of solar UV light when the sun was setting or had just set. The cases chosen were solar zenith angles of 89.9, 93 and 98 degrees. The 98 degree case comes closest to the actual situation. Figure 6 presents the results of these calculations. The onset of 1% transmission for the 98 degrees case is about 3600 Angstrom and by 4000 Angstroms only 2.5% is reaching the missile altitude. This means that the analysis of the night data which are not saturated needs only minor corrections for solar scattering from the plume particles. To first order, the effect can be ignored and a flux level determined just from the plume brightness itself.

Of the two missions, the night data set is the least contaminated by solar radiation scattered from the plume particles. Unfortunately, tracking difficulties and saturated data make the quantitative reduction of this set most difficult.

Figure 7 is the convolution of a blackbody source at 2420 K (the estimated melting temperature of alumina believed to be the principal emitter in the plume) and the wavelength-dependent atmospheric transmission from a source at 40 km altitude to an observer at 11 km altitude, with a slant range of 40 km. The solid line in the top panel represents the blackbody flux, and the

dashed line is the linear representation of the atmospheric transparency. The convolved product of these input functions is given in the middle panel and is indicative of the relative intensity of light reaching the aircraft.

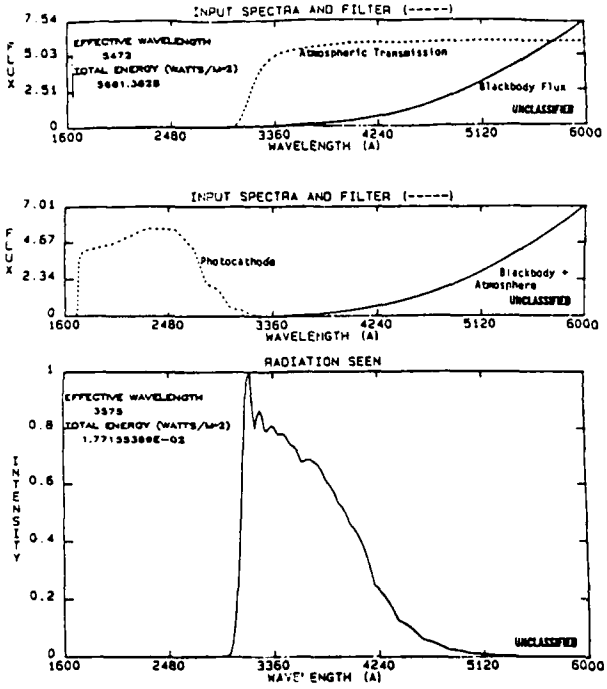

Figure 7. *Convolution of Burning Alumina with* Atmospheric and UV Camera System

The incoming radiation at the aircraft is convolved in the lower panel with the quantum efficiency of the photocathode, which is the principal spectral shaping function for the response of the system shown in the middle panel. The lower panel represents the response of the system to the transmitted blackbody radiation from the missile.

The long wavelength tail in the total response is especially disturbing. Rejection at the red response required additional filtering for future collections.

Chuffing in the Visible and UV in the Night Flight

The night visible data set showed several chuffing events in the early part of the flight. ("Chuffing" is the colloquial term for fluctuations in the plume intensity or shape, often accompanied by ejection of clumps of burning fuel.) In high speed photography, chuffing disturbances can often be seen to move through the plume at about the flow velocity. Similiar effects occur during missile destruction (see Fig. 8). Comparing the visible and UV data, one notes that none of the numerous bright solid propellent chunks seen in the visible images were observed in the UV during the destruct phase. This may impact a visible tracker that might have its centroid shifted or completely redirected. The data from this test imply that tracking in the UV may be unaffected by chuffing.

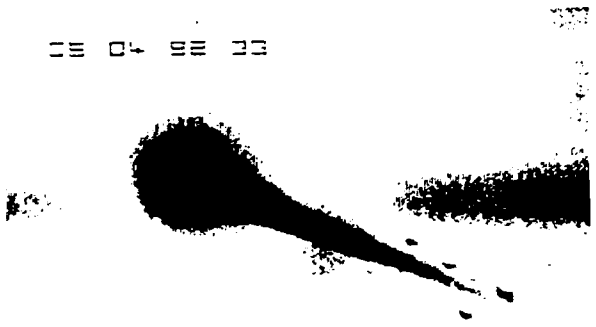

Figure 8. Visible Narrow Field-of-View Image of Night Mission Motor Destruction

Day Second Stage Data

The day flight occured at about noon local time. Unlike the situation for the night launch, the sun was fully illuminating the exhaust plume. In order to estimate the magnitude that the solar scatter masks the intrinsic plume brightness, it is necessary to examine the illumination and observation conditions for the daytime flight. Figure 9 developed the effective spectrum of observed light.

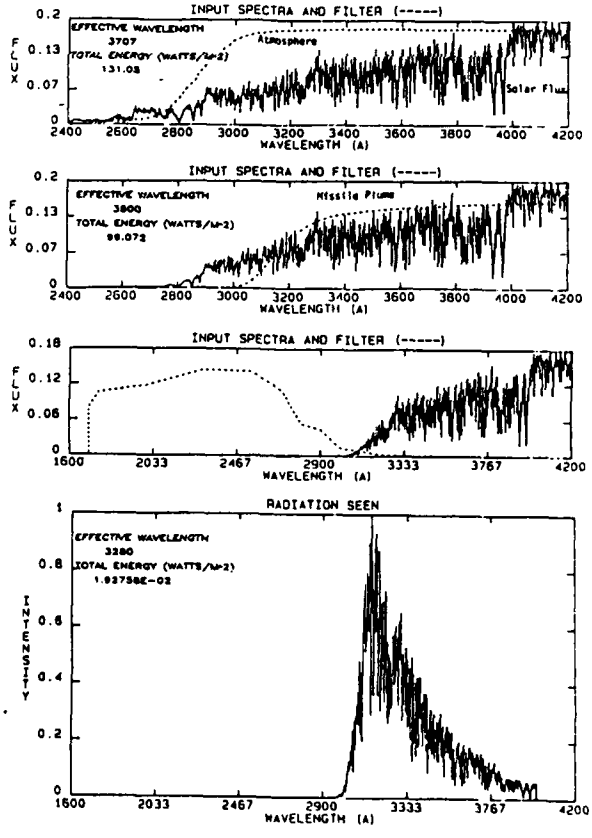

Figure 9. Convolution of Day Plume Radiation with UV Camera

The top panel of Figure 9 shows the unattenuated solar spectral flux (solid line) and the effective transparency of the atmosphere down to the 40 km altitude of the missile (dashed line) for the day mission. The convolved effective solar illumination on the missile is displayed in the second panel.

The second panel represents the second stage in the optical propagation. The panel has the solar illumination of the missile and its plume at the 40 km altitude, as the solid line, and the atmospheric transparency between the 40 km altitude and the aircraft altitude of 11 km is the dashed function. The resultant relative intensity at the aircraft altitude and range is shown in the third panel. A necessary assumption for this analysis step is that the reflection process at the plume is totally neutral, that is, there are no spectral absorptions active (either narrow band or broad band). It is unlikely that this is a correct assumption, but rather sophisticated modelling is needed to generate a proper function. The third panel indicates the relative spectral content of the intensity of light reaching the exterior of the aircraft.

The third panel applies the principal spectral sensitivity function of the camera photocathode-CCD sensor to the incoming radiaton. The solid curve in the third panel is the relative spectral content of the radiation reaching the airplane, and the dashed curve is the camera spectral response. The net effective performance is given in the lower panel. The effective wavelength is around 327 nm, allowing for a small differential wavelength dependent absorption by coatings and optics in the system. Most of the response is between 305 and 345 nm. Future efforts should use a red-end tailoring filter to terminate response at wavelengths longer than 345 nm.

To estimate the reflected solar energy from plume particles, it is necessary to provide a value for the scattering efficiency and make assumptions on the optical thickness of the plume. These two parameters are a detailed study in their own right. We know that the spectral signature of scattering will be dependent upon the particle size. A simple single number is not sufficient to properly address this issue. Similarily, the optical thickness of the plume at several wavelengths in our region of interest (280 - 400 nm) is not a constant. The observed radiation is compared on the solar scatter from the spatially varying particle size distribution, and by the emission of the hot plume particles as they leave the nozzle. There is also a possibility that a hotter source region inside the nozzle can have a single scatter interaction with particles just outside the nozzle to cause observed radiation at an apparent blackbody temperature higher than that of molten alumina particles (about 2420 K).

Visible Data Sets

The visible camera was an ICID television camera sensitive in the visible range with automatic gain control (AGC). As such, quantitative data on photon intensity were not recoverable. However, knowing range, aspect angle, and the camera field of view, an estimate of plume size was possible. One understands that plume size is a function of the threshold selected which, for our case, was an automatic function. Therefore, the sizing is based on the AGC selected near saturation position of the plume without including the less intense portion of the tail. Even with this function, the visible tail was seen to fluctuate upwards of 50 meters in length over only a few frames. The cross axis fluctuation also varied by several meters (up to 5).

RESULTS

Night Mission Results

Selected frames of visible data are shown in Figures 10 and 11. One sees fluctuations in length and width image to image in a nonsymmetrical fashion. Give the variations in length and width, a centroid tracker would jitter the centroid (or hardbody open loop handoff) by several meters with obvious deleterious results.

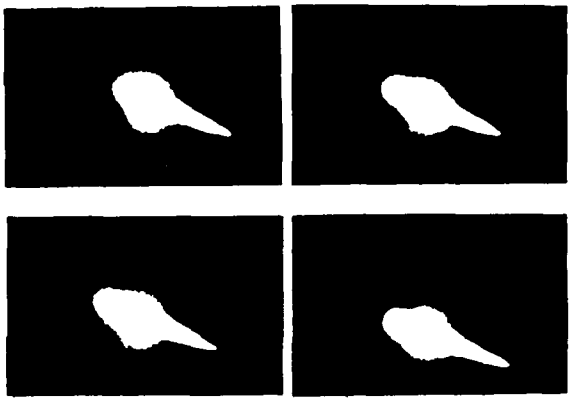

Figure 10. Early 2nd Stage Visible Plumes (Night)

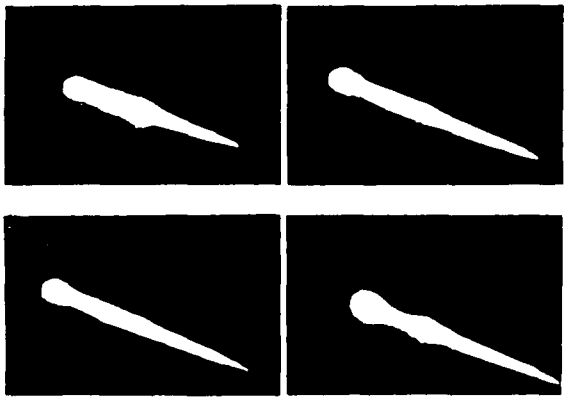

Figure 11. Mid 2nd Stage Visible Plumes (Night)

Figure 12 shows the different between visible and ultraviolet plume sizes for the night mission. Anomalous light sources quench quickly in the ultraviolet and the plume is much better behaved and smaller by at least a factor of two. Filtering the "redtail" of the UV would further reduce the UV plume image in intensity and most probably in size helping to better define the location of the hardbody for tracking.

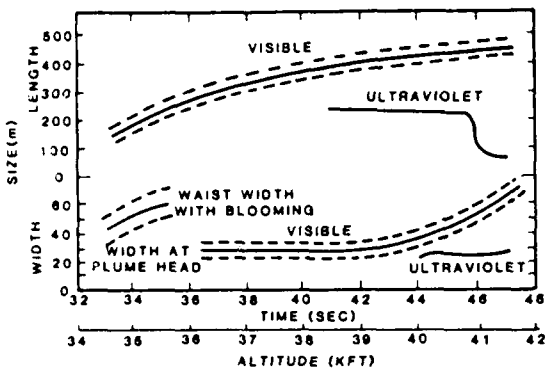

Figure 12. Visible and Ultraviolet Night Plume Size for 2nd Burn (Arbitrary Intensity Threshold

The head of the UV plume grows with altitude as the missile reaches much less dense atmospheric similar to the visible plume. However, the visible tail remains throughout burn unlike the UV where afterburning ceases upon exiting the ozone layer (40.5 Km) of the atmosphere. All this agrees with theory. The increased intensity observed by the UV camera is well accounted for by the "redtail" in the RbTe photocathode.

Subtracting out local background and atmospherics, the night mission ultraviolet radiance is calculated and plotted in Figure 13. In this graph, the most probable radiance is plotted. The radiance is based on a 3300 angstrom center wavelength with ± 100 angstrom bandpass referenced from the photocathode response to the plume emission. For the night mission, the image is saturated, so the average irradiance is a lower limit of actual radiance. The upper two curves depict the radiance of those pixels that are within 90% and 50% of the pixel with the peak radiance. These are an estimate of the peak radiance in the plume (but again, a lower limit, given the saturation). The break in the middle of each plot represents a delay between second stage burnout/destruction and an anomalous apparent burn that remains unexplained.

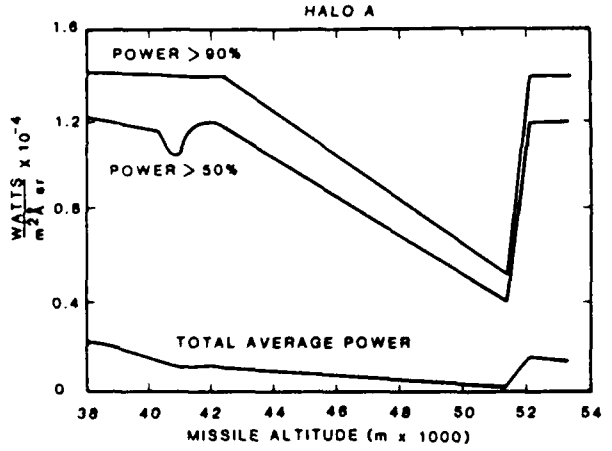

Figure 13. Estimated UV Optical Power Density as a Function of Altitude for Night Mission

Day Mission Results

Selected frames of visible data as shown in Figure 14. There is little fluctuation in length or width due to the solar scatter off the plume particulate. The camera used to take these data was the visible track camera for the narrow field of view UV camera with 5° horizontal field of view. Some interlace effects are noted in the image so sizing the plumes are subject to this error along with the error that comes with the larger field of view.

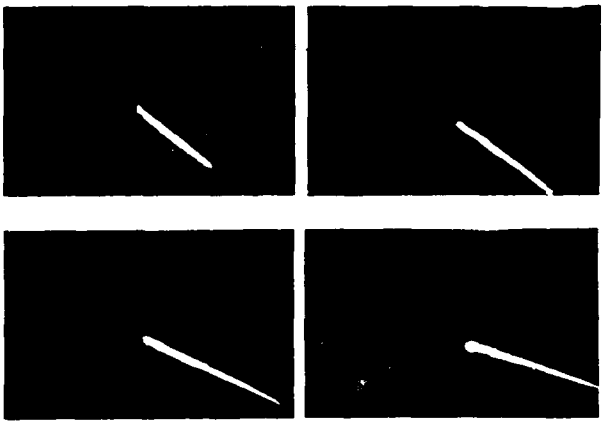

Figure 14. 2nd Stage Visible Plumes (Day)

Figure 15 shows the difference between the visible and ultraviolet plume size for the day mission. The ultraviolet plume is a factor of two smaller than the visible plume but is still quite large.

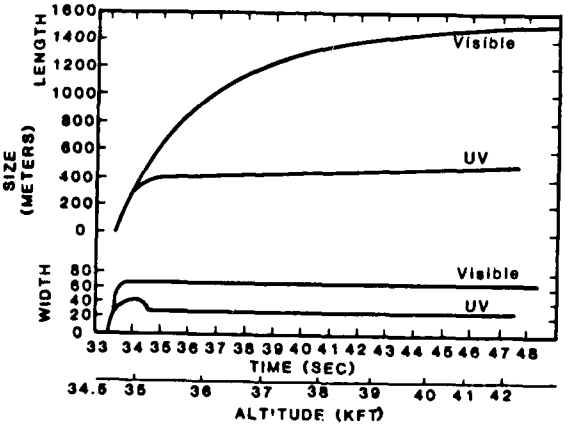

Figure 15. Visible and Ultraviolet Day Plume for 2nd Stage Burn (Arbitrary Threshold)

The day mission maintains a visible plume for upwards of 1500 meters. A centroid tracker handoff to the hardbody of about 750 meters would require error limits of less than 0.1% in distance along the plume just to intersect the hardbody. This is about a factor of four more stringent than the day UV plume and an order of magnitude more stringent than the night UV plume.

Subtracting out local background and atmospherics, the day mission ultraviolet radiance is calculated and plotted in Figure 16. Similarily to the night mission, the uncertainty bounds of -40% to +55% exist. Since there is strong solar glint off of the plume, the plume is much more uniform in intensity and much longer than at night in a similar manner to visible plumes. The day mission was fortunate not to saturate and still capture second stage ignition. Since the first stage was attached to the upper stage until ignition, it can be seen tumbling away in the second stage plume. It determines the plume width for the first couple of seconds until it cools and falls away. This can be seen in the first seven UV data frames, one of which is shown as Figure 17. In the first frame, the 1/60 of the second interlace can clearly be seen from the 1/30 second frame rate in the camera. Here the plume grows at such a rate that we estimate at least 100 hz camera would be necessary to fully capture plume growth.

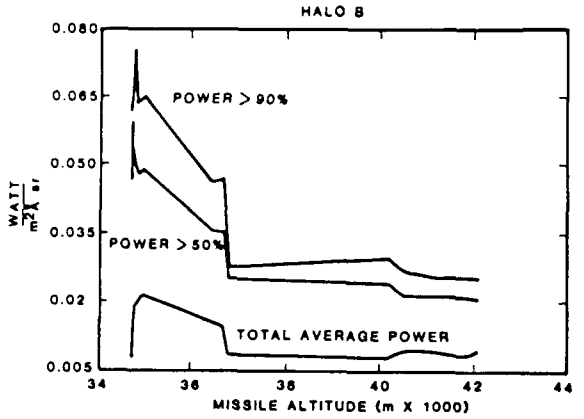

Figure 16. Estimated UV Optical Power Density as a Function of Altitude for Day Mission

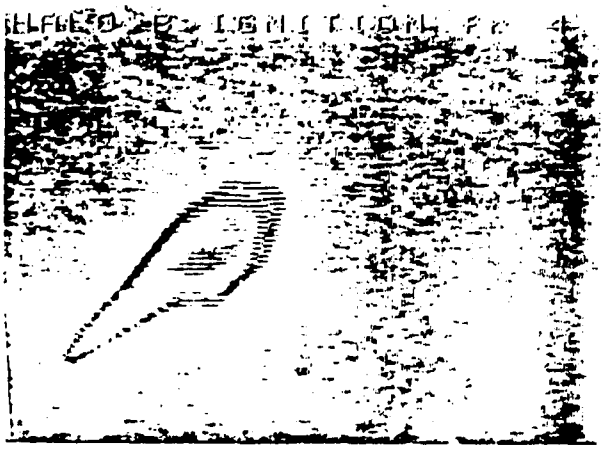

Figure 17. UV Camera Mission Showing Stage Fallaway and Interlacing

Pointing and Tracking Discussion

To estimate the actual track error, the imagery was digitized to a resolution of 256 x 256 pixels with 256 gray levels per pixel (1 pixel = $1/256^2$ Field of View). These imagery data were processed by three different tracker algorithms: a leading edge, a binary centroid (silouette), and an intensity centroid. The imagery was thresholded at 1%, 5%, 50% and 90% of full scale for each of the track algorithms. Track statistics were gathered for each tracker/threshold combination.

The leading edge tracker algorithm used in this analysis determines the outlines of the light/dark discontinuity by differentiation of the light intensity. A priori knowledge fixed the edge in the direction of motion. For aspect angles measured from the tail of 80° to 180°, one expects that the leading edge will be more stable as it is confined by the rocket nozzle. As the aspect angle decreases to zero and the missile gains altitude, the plume expands and obscurs the rocket nozzle from the viewer. Then the leading edge becomes very noisy due to thrust vectoring as well as with the other noise sources in the camera system, atmosphere and algorithm.

A binary centroid tracker algorithm silhouettes the plume and finds the geometric centroid. An intensity centroid tracker weights the silhouette centroid by the light intensity. A priori knowledge fixed the direction of motion for both algorithms. Both trackers integrate over the area to find the centroid areas which average the edge errors, and in turn, yield less noisy data.

Thresholding is a technique that eliminate a portion of the data that is below a percentage of full scale. Thus, a 50% threshold eliminates all data that is below the half intensity level. This action cleans up the image making it "crisper" on the edges and smaller in size such that tracking algorithms can more accurately calculate missile position from trailing plume data.

In the night mission case, the data was predominantly saturated so that there is little change in the picture above 50% thresholding.

A large tracking error was observed in the manual tracks of the missiles for both day and night. Figures 18 and 19 show a 25-35 pixel jitter in both row and column measurements of centroid intensity. Convolving this error with the atmospheric, camera system, and plume motion error leave one with excessive error that cannot be deconvolved for analysis.

Low frequency jitter due the mount, turbulence, and tracker errors will tend to move the entire image. Plume instabilities might affect the shape of the plume, causing the behavior of the leading edge and centroid to differ. Table 2 statistics reflect the noncoherent motion between the leading edge and the centroids. If this indeed is a measure of low frequency plume motion, then it reflects the low frequency incoherent plume motion.

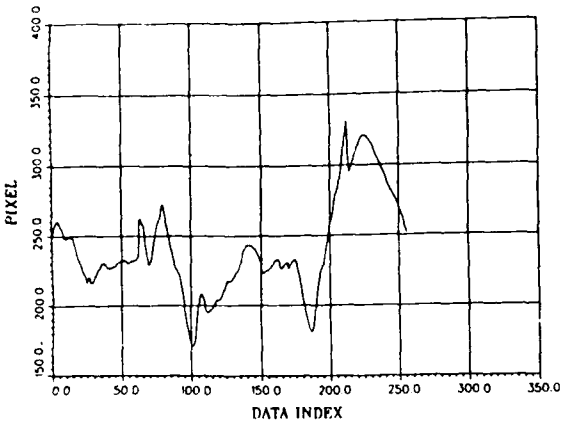

Figure 18. Intensity Centroid Location (Row) Data Index Refers to Individual Sequential Frames

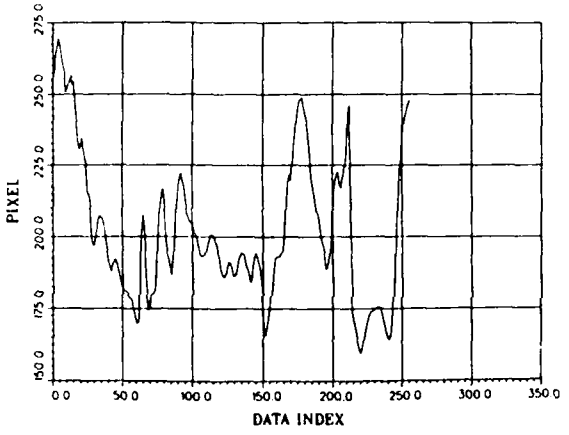

Figure 19. Intensity Centroid Location (Column)

	Threshold							
	1%		5%		50%		90%	
Algorithm	X	Y	X	Y	X	Y	X	Y
Leading Edge	21.2	13.7	21.2	14.6	12.4	16.4	7.8	17.0
Binary Centroid	5.9	8.1	5.8	8.2	5.9	10.1	6.1	9.1
Intensity Centroid	0.7	7.6	0.7	7.5	0.8	7.2	1.2	6.1

Table 2. Image Motion as Measured by Different Track Algorithms (1σ, in pixels)

A measure of the intrinsic plume stability is the relative motion of the plume leading edge to the plume centroid. To study this measure, the difference between the leading edge and centroid errors was computed (see Table 3).

	Threshold							
	1%		5%		50%		90%	
Algorithm	X	Y	X	Y	X	Y	X	Y
Leading Binary	21.0	11.9	21.0	13.1	10.2	14.4	2.6	12.5
Leading Intensity	21.3	12.7	21.3	13.4	12.1	14.4	7.0	14.9

Table 3. Leading Edge Referenced Centroid Track Errors (Pixels)

FUTURE IMPROVEMENT

Blocking Filters and Photocathode Changes

The red tail observed in the data is especially distressing when viewing black body radiation and needs to be removed from the light entering the UV camera on future missions. One approach to this is to construct a special filter that has a drastic cut-off at about 3500 A. Such filters are available. To illustrate the improvement available from this approach, we have constructed an effective performance curve, in the same manner as the performance curves presented above. Figure 20 in the upper panel convolves the 2420 K blackbody emission curve (solid line) with the atmospheric transmission loss from 40 km to 11 km altitude (dashed line). The second panel indicates the resultant relative intensity of radiation reaching the aircraft at its altitude, with a 40 km slant range. Figure 20 (second

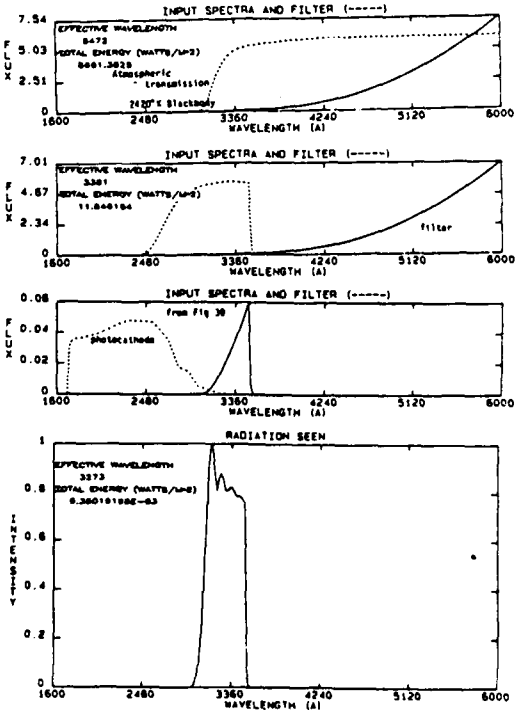

Figure 20. Convolved UV Camera System With Source Radiation

panel) also convolves this input function (solid line) with the transmission characteristics expected from the new filter. The third panel convolves these two functions in the solid line, and clearly shows the proposed improvement.

The final convolution with the present photocathode is given in the lower panel. The third panel shows the filter convolution (solid line) and the photocathode response (dashed line). The resultant performance is in the lower panel and illustrates the superb quality of the proposed filter addition. The total transmission of this filter is greater than 70%, so the losses are not a major issue.

Other Improvements

Other improvement include removing the automatic gain control, and automatically recording the gain while adjusting to eliminate saturation of all data banks. The approach that has been implemented on the UV camera is to insert on the first few (40-55) pixels a gray scale so that the line by line absolute radiometrics is possible. This only shrinks the frame by about 5% and gains a major quantitative factor.

Since superposition of the IRIG time signal onto the data frame has been shown to degrade the data image, IRIG is carried on a parallel voice channel with the obvious drawback of not having IRIG available for single video frames.

Finally, data collection should be accomplished by using a video disk which does not degrade upon replay and captures data at about a 10 Mhz rate which is an order of magnitude better than current U-matic tapes.

CONCLUSIONS

A set of visible and ultraviolet image data has been taken for both day and night backgrounds of a common solid booster upper stage with a limited schedule and budget. Calibrated ultraviolet radiometry was also obtained although much of the data was saturated. Plumes were relatively large and bright although the UV was about 1/2 the size of the visible. Furthermore, anomalous events such as chuffing and quickly varying plume length in the visible were much reduced in the UV. Afterburning outside the ozone region did not appear for the UV.

The rapid quenching of the UV light brought about by rapid cooling of particulates and exiting the upper regions of the atmosphere leads to the conclusion that UV tracking during upper stage thrusting may be more stable than similar tracking in the visible.

The consequences of this type of plume are that a centroid tracker that works well with a round target would be hard pressed to find the centroid position along the plume unless it is tracking the UV plume outside the atmosphere. Thus, other trackers or imagers should be considered were one to track the plume and handoff to the missile in the atmosphere.

Numerous improvements to data collection, handling and reduction have been made as a result of this experiment which portend significant advances in the state of knowledge of plume phenomology and tracker modes.

AVIONICS FOR A FRACTIONATED SLBM

Robert E. Brainard
Lockheed Missiles and Space Company, Inc
Sunnyvale, California

Abstract

Ballistic missile vulnerability to exoatmospheric encounter by space deployed weapons can be significiently reduced by early deployment of reentry bodies. For a Submarine Launched Ballistic Missile (SLBM) the bus can be eliminated and the third stage replaced by third stages attached to each Maneuvering Reentry Body (MARB). This missile configuration requires a different approach to avionic design.

An integrated avionic system is described which provides guidance and control for the booster stages, fractionated third stage and MARB. Avionics include missile electronics located with the booster second stage and guidance and control sensors and electronics located in each MARB.

MARB avionics requires high accuracy and high reliability with severe constraints from available space and the rugged environment. Lack of operational accessibility for repair or replacement demands high reliability.

The guidance and control sensor is a Stellar Inertial Measurement Unit (SIMU). It is a strapdown, configuration which includes a stellar sensor, ring laser gyros and solid state accelerometers.

Technical challanges for avionic contractors are the design and development of a strapdown stellar sensor and solid state accelerometers which can meet requirements for high accuracy and can operate in the rugged environments. Electronic miniaturization also requires innovative design.

Introduction

Current SLBM configurations have three boost stages and a bus. The bus is used to provide precision impact accuracy, footprint capability and precision deployment of multiple independently targeted reentry bodies. The bus operation requires several minutes of time to accomplish its objectives. The bus operating time plus the three stage booster operating time results in reentry body deployment above the Earth's atmosphere where the missile with undeployed reentry bodies becomes vulnerable to exoatmospheric encounter by space deployed weapons. [1,2]

A proposed solution to this problem is to eliminate the bus and replace the third stage with a third stage attached to each reentry body. If the reentry body is a MARB it can correct for third stage propulsion errors and for prelaunch and boost guidance errors which become observable during coast after third stage burnout.

This paper describes a reference missile configuration, addresses the avionic requirement issues and describes an avionic configuration which can meet those requirements.

Design Objectives

Design objectives are to decrease the time after launch for deployment of all reentry bodies while maintaining missile accuracy, range, throw weight, foot print capability and reliability.

Missile Description

A typical SLBM is shown in figure 1. It is a three stage ballistic missile with a bus used for deployment of the reentry bodies. The bus contains the major avionic components including missile guidance, flight control, bus reaction control system, missile electrical interfaces and missile electrical power.

The Fractionated SLBM is also shown in figure 1. It is also a three stage ballistic missile, but the third stage is fractionated and attached to each reentry body. The reentry body is a MARB. The bus has been eliminated. Bus avionics has been redistributed to the missile electronics assemblies attached to the second stage and the MARB avionics.

Avionic Description

The missile electronics contains

- Missile computer
- Interfaces
- Missile electrical power

The missile computer performs guidance and control computations during standby, prelaunch, first stage flight and second stage flight until MARB deployment occurs. Guidance and control navigation data is generated by each MARB avionic system. That data is sent to the missile computer for missile guidance and control computation. The missile computer also controls and responds to the transfer of data between submarine fire control via the missile umbilical and each MARB computer. Missile electronics also contains missile electrical power which includes the missile battery and a power distribution system. The battery provides missile internal electrical power. The power distribution system controls the availability of missile internal and external power and MARB external power.

MARB avionics include

- Stellar Inertial Measurement Unit (SIMU)
- Electronics
- MARB electrical power

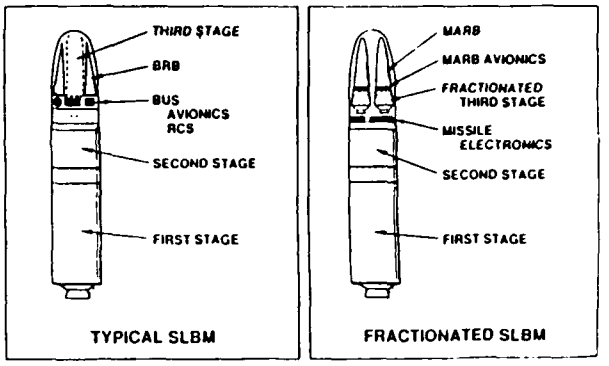

Figure 1 SLBM Configurations

SIMU is a strapdown, solid state configuration which contains the stellar sensor, ring laser gyros and accelerometers. A strapdown configuration is preferred rather than a gimbaled platform. A strapdown configuration can be designed to meet the accuracy requirements and can more easily meet the severe volume and shape requirements imposed by a MARB installation. Smaller volume also reduces weight for increased performance. Solid state sensors are preferred in order to meet system reliability objectives. Solid state sensors also have better input sensing axis stability, which is another important accuracy consideration.

The stellar sensor is required to maintain SLBM accuracy by providing precision attitude measurement data during coast. The stellar sensor improves system accuracy by reducing the contribution of initial condition errors from longitude and latitude position and azimuth angle. Initial condition values for longitude, latitude and azimuth are obtained from the submarine Ship Inertial Navigation System (SINS). The strapdown stellar sensor accuracy has to be equivalent to the current SLBM SIMU stellar sensor accuracy if SLBM accuracy is to be maintained.

Ring laser gyros can meet the attitude stability, reliability and operational life time requirements. The major design issue is to meet the required performance with the smallest configiration integrated into the SIMU.

Accurate solid state accelerometers capable of performing in the reentry deacceleration

environment are required. The Kearfott Vibrating Beam Accelerometer (VBA) has the required performance. [3] However, further development is required to meet the combined requirements of high accuracy and reentry deacceleration levels. Silicon accelerometers currently do not have the required accuracy.

MARB electronics must implement the required functions efficiently and meet the requirements for small size and shape, low power and high reliability while meeting the design requirements for reentry radiation hardness levels and the rugged environments of shock, deacceleration and thermal. Low power results in a smaller battery, higher reliability at lower temperature and simpler, lighter weight methods for heat dissipation. Small size and lower power also reduces electronic weight.

Electronic parts must maximize the use of Very High Scale Integrated Circuits (VHSIC) and hybrid modules. Package design must emphasize minimum volume and shape configuration consistant with high reliability, producibility and maintainability.

The MARB electrical power system includes a squib activated silver, zinc battery and an external, internal power distribution system.

Flight Sequence

The flight sequence is illustrated in figure 2. During prelaunch, target data from fire control can be updated, navigation initial conditions are provided, and the component of combined longitudinal accelerometer bias and scale factor is estimated for each MARB SIMU. The navigation initial condition data is obtained from SINS. This includes longitude, latitude, height, azimuth, and velocity.

During first and second stage flight, the missile computer will process the MARB navigation data from each MARB to determine a best estimate of navigation data for boost guidance and control. By processing all available MARB navigation data, mission accuracy and reliability is enhanced.

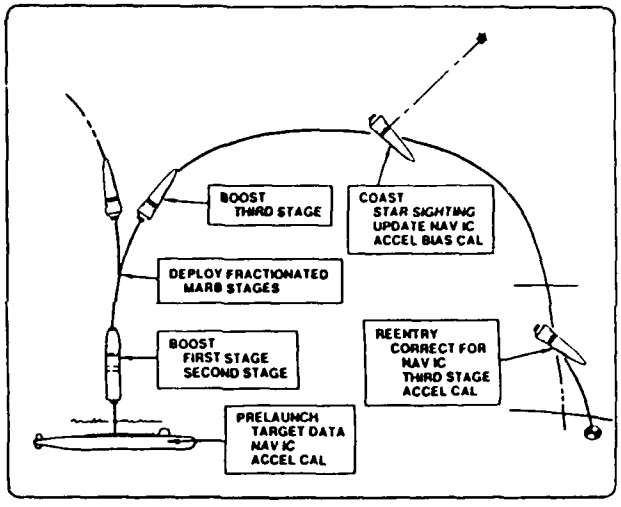

Figure 2 Flight Sequence

MARBs, with an attached third stage, are deployed during second stage burn, or shortly after its burnout. The deployed MARB will then correct its attitude, with its reaction control system, followed by third stage ignition. After third stage burnout, errors associated with third stage burn are determined from the navigation data. Third stage errors can be caused by nonnominal performance of the propulsion system and attitude control.

During coast, after third stage burnout, the MARB attitude control system will reorient and stabilize the vehicle attitude to obtain at least two, noncollinear, star sightings. Star sightings will continue during coast, unless interrupted by temporary hostile encounters which the avionic system survives. Also, during coast, accelerometer bias is estimated. This data, combined with the prelaunch estimate of the longitudinal combination of accelerometer bias and scale factor, permits the separation of longitudinal accelerometer bias and scale factor which then results in an updated estimate of longitudinal accelerometer scale factor, as well as accelerometer bias.

During reentry, the MARB can maneuver to correct for accumulated navigation errors,

including third stage errors, corrections from star sightings and preflight and inflight estimates of accelerometer bias and longitudinal scale factor. The MARB is also available to perform other operational maneuvers during reentry.

Reliability Issues

As a design objective, missile reliability is to be maintained. The Fractionated SLBM configuration has major avionic components installed in each MARB. These components are not physically accessible for repair or replacement while the MARB is installed in the missile while in the submarine launch tube. Consequently, the standby, or dormant, reliability of the avionic components must be very high.

Periodic testing with built-in-self-test (BITE) will be performed to determine the existence of disabling failures in the MARB avionics. Because MARB avionics provide redundent guidance and control navigation data for the first two stages of the missile, it can still be launched when MARB avionic failures have been detected. The missile guidance will be designed to operate in the presence of failed RB avionics and still meet safety requirements. It is of course prudent to repair that missile at the earliest opportunity.

To achieve high reliability, design simplicity, minimum parts, an effective parts reliability program and component burn-in are required. System design must achieve low power, with efficient heat dissipation to minimize operating temperature. The design must be constrained for power off during standby to minimize the initial starting temperature and contributions from the higher failure rates associated with energized conditions. Of course, these reliability design constraints and objectives can make attainment of accuracy objectives more difficult. The selection of the strapdown, solid state, and miniature electronic design approach is intended to meet the reliability design constraints and objectives as well as the functional and accuracy requirements.

Available Technology

Avionic technology which is available for implementation of the Fractionated SLBM design are

- Flight computers
- Miniature, low power electronics
- Hardened digital electronics
- X ray shielding
- Ring laser gyro
- High reliability with restricted maintenance constraints

Lockheed Missiles and Space Co., Inc (LMSC) is developing a radiation hardened computer which can perform the required computations for the missile computer and the MARB computer. This computer can meet reentry radiation hardness levels. It has a throughput capability of 5 million instructions per second (mips). It is compatible with high level languages, including ADA, for cost effective firmware development and maintenance. This computer has such a high capability that the specific design of operational algorithms become less critical in the sense that creative design compromises to minimize throughput and memory storage are not major design drivers.

Radiation hardened, low power electronics can be miniaturized by using VHSIC, CMOS/SOS, hybrid chip modules and innovative packaging design. X ray shielding designs and radiation hardened digital parts are available.

Strapdown ring laser gyros are being used in many applications. Accuracy, low power, high reliability and radiation hardness are available features. Designs with smaller size and shape with higher performance are becoming more readily available.

Currently available reliability capability can satisfy the Fractionated SLBM design constraints and meet reliability requirements. Selected reliability features include strapdown, solid state sensors, solid state digital electronics, effective part reliability programs, component burn-in and understanding of part failure mechanisms with effective design corrective action.

Advanced Technology

The Fractionated SLBM design requires advanced technology which includes

- Strapdown stellar sensor
- Solid state accelerometers
- Hardened analog electronic parts
- Flight computer memory

The most critical advanced technology avionic component is the strapdown stellar sensor. It must provide accuracy equivalent to the present SLBM stellar sensor, which is mounted in an accurately controlled thermal environment within an inertial attitude stabilized gimbaled platform. A nontemperature controlled environment plus the compromising vehicle inertial attitude rates sensed by the strapdown configuration impose special design requirements on strapdown stellar sensor sensitivity, response time and data processing requirements.

Solid state accelerometers are currently in an advanced state of development. The Kearfott VBA is an excellent candidate. However it must meet the required accuracy requirements and still perform in the reentry deacceleration environment. The currently projected accuracy of solid state silicon accelerometers do not meet the required accuracy.

Strapdown stellar sensors and solid state accelerometers require dedicated advanced development programs.

Development needs to continue of radiation hardened analog parts in order to meet reentry levels. Critical part types include operational amplifiers and voltage references.

Flight computer memory must be radiation hard, small, fast and power efficient. Emerging candidates are State Retention Memory implemented with CMOS/SOS and Ferroelectric memory.

Conclusion

To reduce SLBM vulnerability to exoatmospheric encounter by space deployed weapons a missile configuration has been defined which significantly reduces reentry body deployment time. The configuration includes a fractionated third stage, an integrated missile avionic configuration and a MARB for subsequent correction of midcourse determined navigation errors. Avionics include a strapdown, solid state SIMU for each MARB. The SIMUs are the source for navigation data used for guidance and control of the boost stages, fractionated third stage and MARB. The required technology is available. However, the strapdown stellar sensor, solid state accelerometers, and electronics require advanced development.

References

1. Dietz, R.C. "Fast Burn Missile Requirements Analysis" LMSC 8171/157, Ballistic Missile Future Systems and Technology Workshop, AFBMO, April 1986

2. Dietz, R.C. "Post Boost Vehicle Design in the Future" LMSC 8171/157, AIAA Future Systems Workshop, AFBMO, MARCH 1988

3. Albert, W.C., Weber, R.E. "Vibrating Beam Accelerometer for Strapdown Applications" IEEE CH1820, 1982

4. Kancler, H.C. "VLSI Rad Hard Computer" LMSC 8160/157

AVIONICS
FOR A FRACTIONATED SLBM

Robert E. Brainard
Lockheed Missiles and Space Co., Inc
Sunnyvale, California

INTRODUCTION

THREAT

- BALLISTIC MISSILES WHICH DEPLOY REENTRY BODIES
  - SEVERAL MINUTES AFTER LAUNCH
  - ABOVE THE ATMOSPHERE
  - ARE VULNERABLE TO SPACE WEAPONS

SLBM SOLUTION

- DEFINE SLBM AND AVIONIC CONFIGURATION
  - EARLY REENTRY BODY DEPLOYMENT
  - MEETS CURRENT SLBM PERFORMANCE
    - ACCURACY, RANGE, THROW WEIGHT, RELIABILITY
    - INCREASES FOOT PRINT CAPABILITY
- AVIONIC DESIGN ISSUES
- AVAILABILITY OF AVIONIC TECHNOLOGY

SLBM CONFIGURATIONS

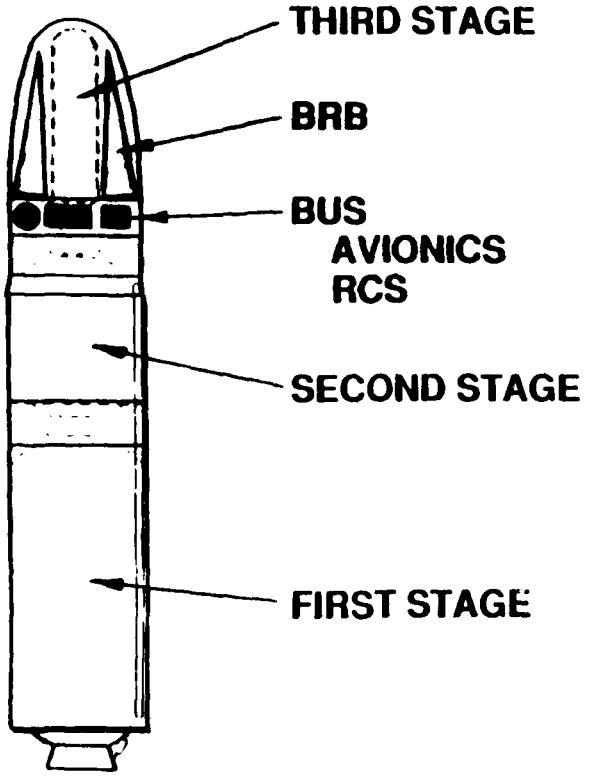

TYPICAL SLBM

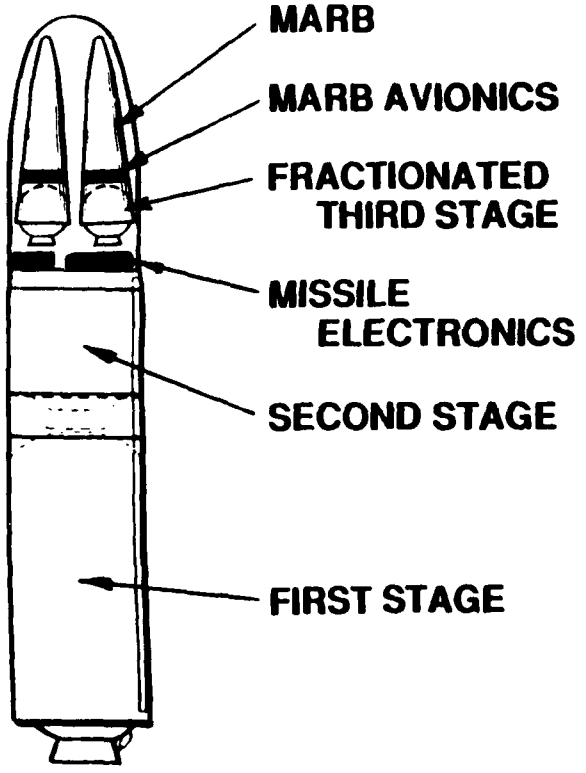

FRACTIONATED SLBM

AVIONIC CONFIGURATION

MISSILE ELECTRONICS

- MISSILE COMPUTER
  - MISSILE GUIDANCE AND CONTROL
  - MANAGES INTERFACE DATA
    - UMBILICAL
    - MARB COMPUTER
- INTERFACES
  - MISSILE RCS AND TVC
- ELECTRICAL POWER
  - MISSILE BATTERY
  - POWER DISTRIBUTION

AVIONIC CONFIGURATION

MARB AVIONICS

- STELLAR INERTIAL MEASUREMENT UNIT (SIMU)
  - STRAPDOWN CONFIGURATION
  - STELLAR SENSOR
  - RING LASER GYROS
  - ACCELEROMETERS
    - SOLID STATE
  - ELECTRONICS
- MARB ELECTRONICS
  - MARB COMPUTER
    - NAVIGATION
    - MARB GUIDANCE AND CONTROL
    - MISSILE INTERFACE DATA
- INTERFACES
  - MARB RCS AND TVC

FLIGHT SEQUENCE

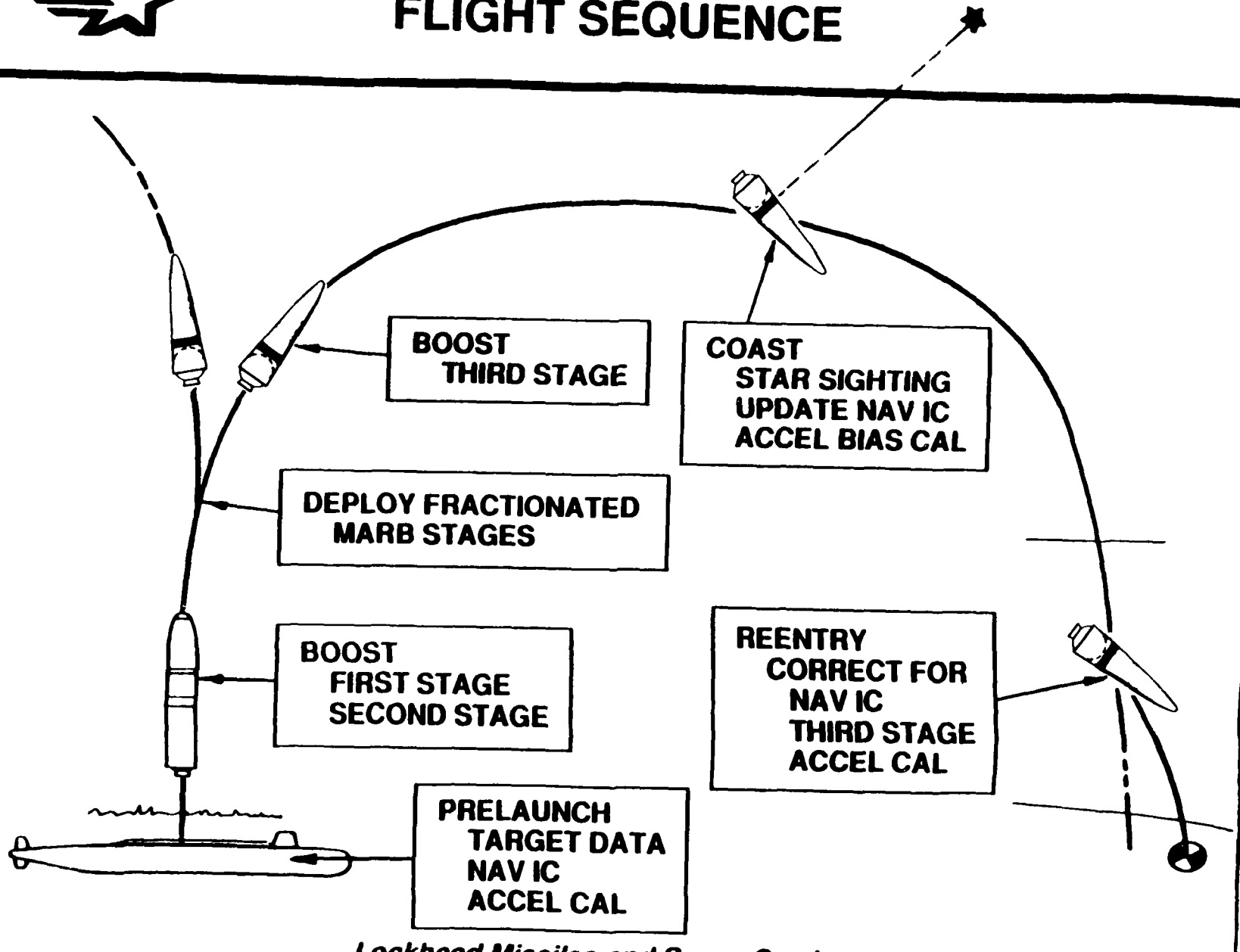

RELIABILITY ISSUES

- DESIGN OBJECTIVE
  - MAINTAIN MISSILE AVIONIC RELIABILITY
  - 3 - 5 YEAR CONTINUOUS SERVICE IN SUBMARINE
    - WITHOUT MAINTENANCE
  - 25 YEAR SERVICE LIFE
- DESIGN CONSTRAINTS
  - MARB AVIONICS ARE NOT ACCESSABLE
    - WHILE MARBS ARE INSTALLED IN SUBMARINE
- THIS REQUIRES HIGH RELIABILITY
- DESIGN APPROACH
  - DESIGN SIMPLICITY
  - MINIMUM PARTS
  - PARTS RELIABILITY PROGRAM
  - COMPONENT BURNIN
  - LOW POWER
    - LOW TEMPERATURE
  - POWER OFF DURING STANDBY
    - HIGHER DORMANT RELIABILITY
  - BUILT IN SELF TEST (BITE)

AVAILABLE TECHNOLOGY

- FLIGHT COMPUTER
  - LMSC DESIGN
    - RAD HARD, VHSIC, CMOS/SOS
    - 5 MIPS
    - HIGH LEVEL LANGUAGE, INCLUDING ADA
- MINIATURE, LOW POWER ELECTRONICS
- RAD HARD DIGITAL ELECTRONICS
- X RAY SHIELDING
- RING LASER GYRO
- DESIGN AND TEST FOR HIGH RELIABILITY
  - OVERCOME ACCESSABILITY CONSTRAINTS
  - 3 TO 5 YEAR STANDBY DORMANCY

ADVANCED TECHNOLOGY

REQUIRES ADVANCED DEVELOPMENT

- STRAPDOWN STELLAR SENSOR
  - HIGH ACCURACY
  - STRAPDOWN ENVIRONMENT
    - BODY RATES
    - THERMAL DESIGN RESTRICTIONS
  - SENSOR SENSITIVITY, RESPONSE TIME, DATA PROCESSING
- SOLID STATE ACCELEROMETERS
  - KEARFOTT VIBRATING BEAM ACCELEROMETER (VBA)
    - MEETS ACCURACY REQUIREMENTS
    - INCREASE ACCELERATION CAPABILITY
      - 200 G DURING REENTRY

ADVANCED TECHNOLOGY

CONTINUE DEVELOPMENT

- RADIATION HARDENED ANALOG ELECTRONIC PARTS
  - REENTRY LEVELS
  - OPERATIONAL AMPLIFIERS
  - VOLTAGE REFERENCE
- FLIGHT COMPUTER MEMORY
  - RADIATION HARD
  - SMALL
  - FAST
  - LOW POWER
  - STATE RETENTION MEMORY
  - FERROELECTRIC MEMORY

CONCLUSION

- DEFINED FRACTIONATED SLBM CONFIGURATION
  - THIRD STAGE ATTACHED TO EACH MARB
  - PROVIDES FOR EARLY MARB DEPLOYMENT
    - REDUCES VULNERABILITY TO SPACE WEAPONS
- DEFINED INTEGRATED MISSILE AVIONIC SYSTEM
  - MISSILE ELECTRONICS
  - MARB AVIONICS
    - STRAPDOWN - STELLAR INERTIAL MEASUREMENT UNIT
      - STELLAR SENSOR
      - RING LASER GYROS
      - SOLID STATE ACCELEROMETERS
- ADVANCED TECHNOLOGY DEVELOPMENT
  - STRAPDOWN STELLAR SENSOR
  - SOLID STATE ACCELEROMETERS
  - RAD HARD, MINIATURE, LOW POWER ELECTRONICS

A RING LASER GYRO BASED STELLAR AIDED INERTIAL NAVIGATION SYSTEM

Shing Peter Kau and John Abernathy

Space and Strategic Avionics Division,
Honeywell Inc, Clearwater Florida

Abstract

This paper presents the concept for several stellar aided Ring Laser Gyro (RLG) Inertial Measurement Unit (IMU) systems suitable for ballistic missile guidance applications. Top level design trade-off analysis results for configurations ranging from pure strapdown to two-axis gimbaled strapdown mechanizations are presented. System mechanization features overcoming the constraints of a strapdown configuration for observability of online determination of key sensor calibration and alignment parameters are described. Stellar aiding relaxes the accuracy required of preflight azimuth alignment. The unparalleled scale factor performance of the RLG offers new flexibility in star sighting strategy. In addition, the RLG offers cost and reliability advantages over conventional gyros.

1. Introduction

The key performance parameters for a ballistic missile guidance system are preflight azimuth alignment and thrust acceleration measurement during the boost flight. These translate into gyro drift and accelerometer scale factor as the critical IMU performance parameters. Current systems require elaborate inertial sensor and platform system designs, and complex preflight flight calibration and alignment operations are performed to accomplish and maintain the accurate azimuth alignment and accelerometer scale factor calibration. The stringent CEP accuracy required of the strategic weapon system has driven up the complexity and cost of booster inertial guidance systems mechanized using conventional spinning mass gyro and stabilized platform technologies. Cost escalations also result from the reliability and maintainability problems that may arise through the life time of such systems where continuous active operation is necessary to maintain the critical thermal environment required for achieving the CEP accuracy.

Stellar aiding can provide the required total system accuracy with greatly relieved IMU requirements. Even with a conventional technology IMU, this relaxation is translated directly into significant cost savings. The accuracy of stellar aiding has been verified in Navy systems and more recently in the flight tests of the GE AINS (Alternate Inertial Navigation System) as part of the USAF SICBM program. For these systems the star sensor is placed in the inner element of a gimbaled platform. The inner element is inertially stabilized during the boost flight with the star sensor LOS pointing in the direction anticipated for a single optimal star sighting.

The development of RLG systems for strategic weapon systems application by the Air Force Ballistic Missile Office has been underway for twelve years. The Honeywell Dormant Inertial Navigation System (DINS) program demonstrated strapdown RLG navigation for maneuvering reentry vehicles.The Alternate Inertial Navigation System (AINS) provided RLG performance improvements and nuclear hardening. The second Generation RLG strapdown IMU is been developed on the current Honeywell Advanced IMU (AIMU) program.

The development of Ring Laser Gyro systems and the stellar sensor offers new flexibility in the design of a stellar aided IMU with attending accuracy, cost and reliability benefits. Due to the absence of moving parts, the RLG strapdown IMU mechanization is inherently lower cost and more reliable than a stabilized platform system using conventional spinning mass gyros. The unparalleled scale factor performance of the RLG provides accurate measurement of angular rotations. The star sensor LOS can be maneuvered to actively seek out any pair of bright and isolated stars with adequate angular separation to acquire complete three axes attitude information for stellar aiding without being constrained by the target position. In addition, a 180-deg roll about the LOS to the star can be performed as part of the sighting maneuver to enable the inflight calibration of the star sensor LOS with respect to the IMU sensitive axis. The excellent gyro scale factor performance ensures the preservation of the star sighting accuracy throughout the large angle maneuvers.

The pendulus accelerometers are typically of small size, low cost and high reliability. The bias and scale factor stability is moderate over the long term. However, over the short term on a continuous operating basis, they are excellent making them suitable for applications where online calibration is available. As a minimum, they are suitable for measurement of applied acceleration on the missile pitch and yaw axes where the performance sensitivities are low. High performance accelerometers, e.g. SFIR, offering excellent long term bias and scale factor stability and modelability, are suitable for measurement of applied acceleration on missile roll axis, the nominal thrust axis. This becomes necessary when online calibration is not available. Under development are vibrating beam accelerometers with potentials of high performance, low cost and high reliability. They are candidates for thrust axis application when the technology matures.

This paper presents the concept for several stellar aided RLG IMU systems suitable for ballistic missile guidance applications. Top level design trade-off analysis results for configurations ranging from pure strapdown to two-axis gimbaled strapdown mechanizations are presented. System mechanization features overcoming the constraints of a strapdown configuration for observability of online determination of key sensor calibration and alignment parameters are described. This assures the high accuracy required for strategic booster guidance applications.

Variations of the aiding mechanization options are presented suiting the capability of the missile vehicle to which the system is applied. This includes providing the environment for online accelerometer calibration, performing the maneuver for star acquisition, and correcting the missile trajectory for the navigation errors determined from online calibration and stellar aiding. Modern missile systems, e.g. Minuteman III, Peacekeeper and Trident, are equipped with a post boost propulsion system capable of fully supporting these operations. Older existing systems, e.g. Minuteman II, do not include a post boost stage. Simplified operations conforming to the constraints on vehicle capability can be performed. System accuracy reduced from the full potential but satisfying the original weapon system requirements can be achieved.

2. System Configurations

Four system configurations are considered in the concept evaluation of stellar aided RLG IMUs as depicted in the geometry presented in Figure 2-1. All four configurations assume the Advanced Inertial Measurement Unit (AIMU) presently in development under Ballistic Missile Office (BMO) contract. The AIMU program has the objective of developing an RLG strapdown IMU with the Inertial Sensor Assembly (ISA) ready for strategic system applications. In increasing complexity, the systems are:

(1) (SD/3A): A pure strapdown mechanization in which the AIMU and the star sensor are mounted fixed to the vehicle

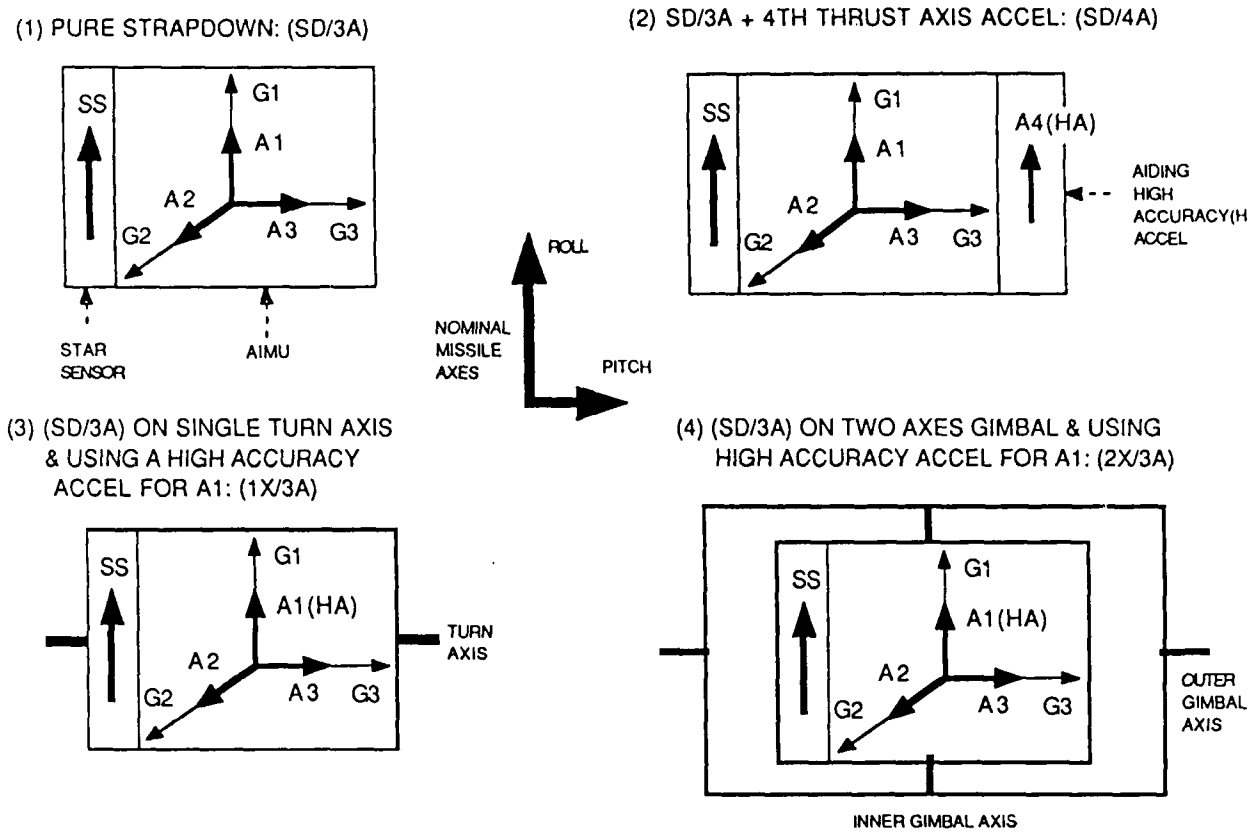

Fig. 2–1. System Configurations for Stellar Aided AIMU

body frame in such a manner that the Input Axis (IA) of one of the three accelerometers is aligned with the nominal missile thrust axis. The strapdown configuration has the advantage of system simplicity with attendant cost and reliability benefits. A vehicle attitude maneuver is required to provide the necessary angular motion and orientation for star sightings. Vehicle body rotation about LOS to a star is performed to allow calibration of the star sensor to IMU sensitive axes alignment. Data processing, correlating accelerometer data from preflight (1–g) and post boost free fall (0–g) measurements provides for calibration update.

(2) (SD/4A): A system consisting of the strapdown system of (1) augmented with a 4th strapdown accelerometer with its IA nominally aligned with the missile thrust axis. A high performance accelerometer, e.g. SFIR, with good bias and scale factor stability and nuclear hardening characteristics is chosen as the 4th accelerometer to aid the thrust axis pendulus accelerometer in the AIMU ISA. Vehicle attitude maneuvering is required for star sighting as in case (1) along with the accelerometer calibration updates.

(3) (1X/3A): A strapdown system with a high accuracy accelerometer in the thrust axis and a single ± 180 deg turn axis. The turn axis is nominally aligned with the missile pitch axis to provide the capability to position the IA of the thrust axis accelerometer up and down during the preflight operation. The turn axis will be controlled during the boost flight with the IA of the thrust axis accelerometer aligned to the nominal missile thrust axis. The re–orientation capability enables the calibration of the thrust axis accelerometer bias and scale factor during the preflight operation and reduces vehicle attitude maneuvering required for star sightings. Full attitude maneuvering is still required for star sensor LOS calibration.

(4) (2X/3A): A system consisting of the strapdown system of (2) placed in the inner element of a two axes gimbal. The rotational freedom enabled by the gimbal provides the complete IMU calibration observability during the preflight operation. It also allows the star sightings to be accomplished with minimum requirement of vehicle maneuver. Two configuration variations are considered in this paper. First, the AIMU ISA is retained with the star sensor LOS parallel to but not coincident with the gimbal axis. The rotation about star LOS will be performed as part of the star sighting maneuvers. Second, the star sensor LOS is parallel to and coincident with the inner gimbal rotational axis. The star sensor LOS to IMU alignment can be accomplished preflight by rotating about the LOS to a case fixed point source.

3. Description of System Operations

The accuracy of a stellar aided system is derived from supplementing the preflight alignment with highly accurate attitude updates available from inflight star sightings. The RLGs with excellent scale factor accuracy enable the use of large angle maneuvers for star acquisition and LOS to IMU calibration while still preserving the basic accuracy associated with the star sightings. However, the stellar aiding does nothing to improve the scale factor performance of the thrust axis accelerometer, the other critical performance parameter for the ICBM boost guidance IMU. This is accomplished through observing accelerometer measurements in the preflight one–g environment and during the post boost zero–g environment. If the post boost zero–g environment is not available, the ability to point the IA up and down in the preflight one–g environment is essential to provide the calibration observability for separation of the accelerometer bias and scale factor errors. System operations during the preflight, boost and post boost mission phases are depicted in Figure 3–1, and discussed in the following.

(1) Preflight: Alignment and calibration updates are performed preflight.

For the pure strapdown system, coarse preflight azimuth alignment is performed along with a lumped parameter calibration of accelerometer bias, scale factor and IA misalign-

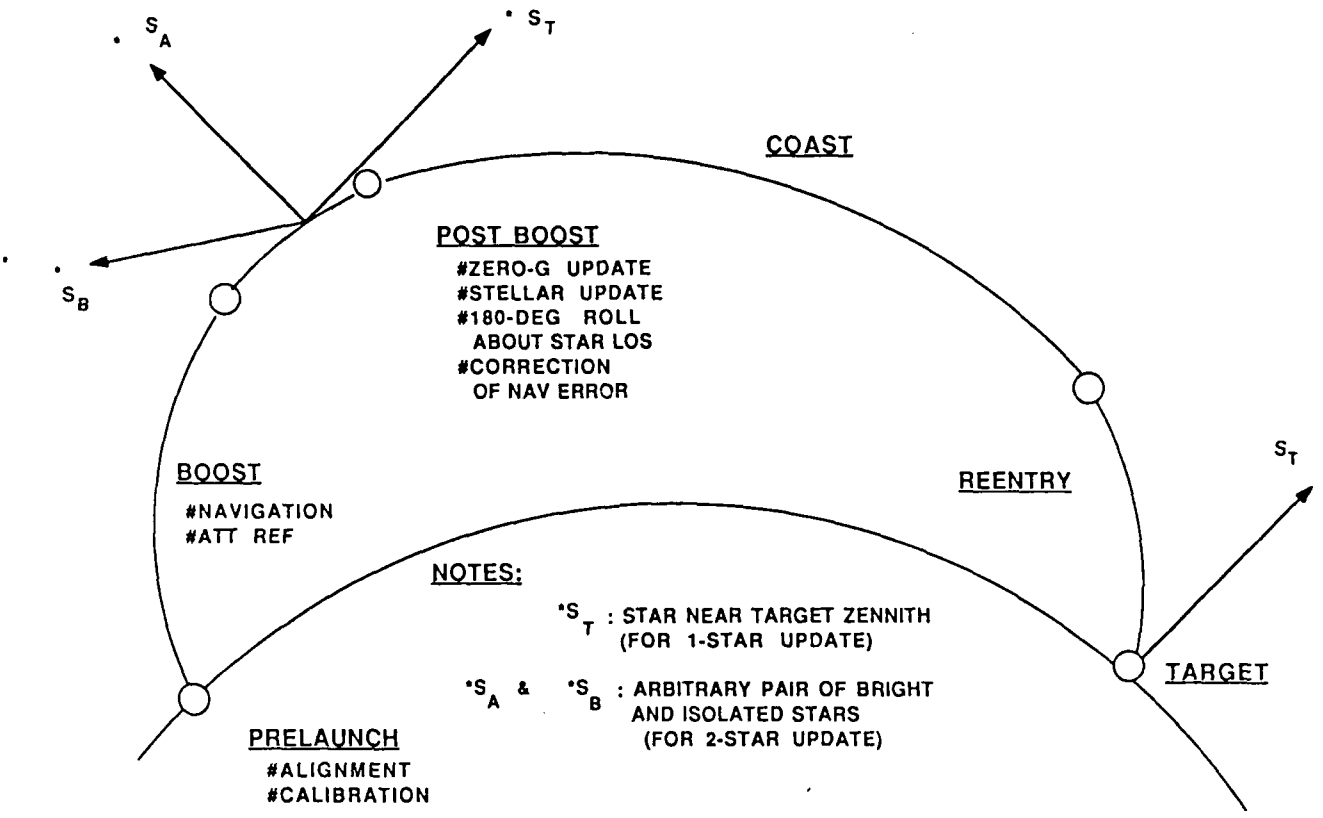

Fig. 3–1. Stellar Aided IMU System Operations

ment errors. No separation of these parameters is obtained.

For the system with a single turn axis, the thrust axis accelerometer will be reoriented during the preflight operation to provide IA–up and IA–down measurements for accurate determination of bias and scale factor.

For the system equipped with a two axes gimbal, complete calibration update of gyro and accelerometer bias, scale factor and input axis misalignment is performed preflight. Since laser gyro bias, scale factor and IA alignment are typically long term stable, a simple calibration profile can be utilized for fast calibration of accelerometer parameters.

In addition, preflight calibration of star sensor LOS to gyro and accelerometer input axes can also be performed using a simulated star fixed to the IMU case. The inner element will be rotated about the inner gimbal axis. The LOS to the simulated star is nominally horizontal to allow varying projections of gravity to the pitch and yaw accelerometers for enhanced calibration observability. This is possible, however, only for the system configuration where the star sensor LOS is coincident to the inner gimbal axis.

(2) Boost: Strapdown attitude reference and navigation functions are performed during boost. For the single axis and gimbaled system, the axes are locked during the boost to function as a strapdown inertial navigation system.

(3) Stellar Update: The update is performed using sightings to one or two stars. If a single star is used, an optimal star providing maximum navigation accuracy is selected. For a two–star sighting, any two bright and isolated stars with adequate angular separation will be selected, subjected to viewing constraints imposed by availability and interference from sun and earth. For the strapdown systems, the star sighting is accomplished with vehicle maneuvers. To update alignment between the star sensor LOS and the IMU sensitive axes, a 180–degree roll about the LOS to the star is performed in between sightings to the same star as depicted in Figure 3–2. For the single axis system the stellar sighting is accomplished using vehicle roll maneuvers and the system axis of turn about vehicle pitch. For the gimbaled system, the star sighting maneuvers are accomplished using the two–axis gimbal. If sightings to a case fixed simulated star is performed preflight, the 180–degree roll about the star LOS need not be performed post boost.

(4) Post Boost Zero–g Update: The update is performed during the post boost free fall for the pure strapdown system. This complements the preflight measurements to complete the calibration observability of the thrust axis accelerometer. In the presence of vehicle angular motion during free fall, the off–CG location of the accelerometers have to be accounted for in the zero–g update processing. The zero–g update is not needed for the gimbaled system, nor for the system with the single turn axis.

4. Performance Evaluation

The performance analysis is evaluated for the purposes of exploring the accuracy potentials of various combinations of the system configurations and mechanization options presented in this paper, and identifying the major error sources involved. These mechanization options represent varying degrees of demand on vehicle capabilities in terms of providing the zero–g environment, performing the maneuvers for star acquisition, and for correcting the missile trajectory for the navigation errors determined in the inflight updates. These are readily accomplished if a post boost propulsion vehicle or a maneuverable reentry vehicle is available. Analyses are performed to evaluate mechanizations where these capabilities are not available, e.g. MM II. The effects of not performing the zero–g update and simplified stellar aiding procedures are evaluated. An error budget based on the performance characteristics of current RLG, accelerometer and star sensor technology is used for system modeling. A typical three staged missile trajectory with 6000 n.mi. range is used for performance evaluation. For analysis purposes, two stars are chosen with the first located on target zenith and the LOS to the second normal to that of the first. The zenith star is always used if

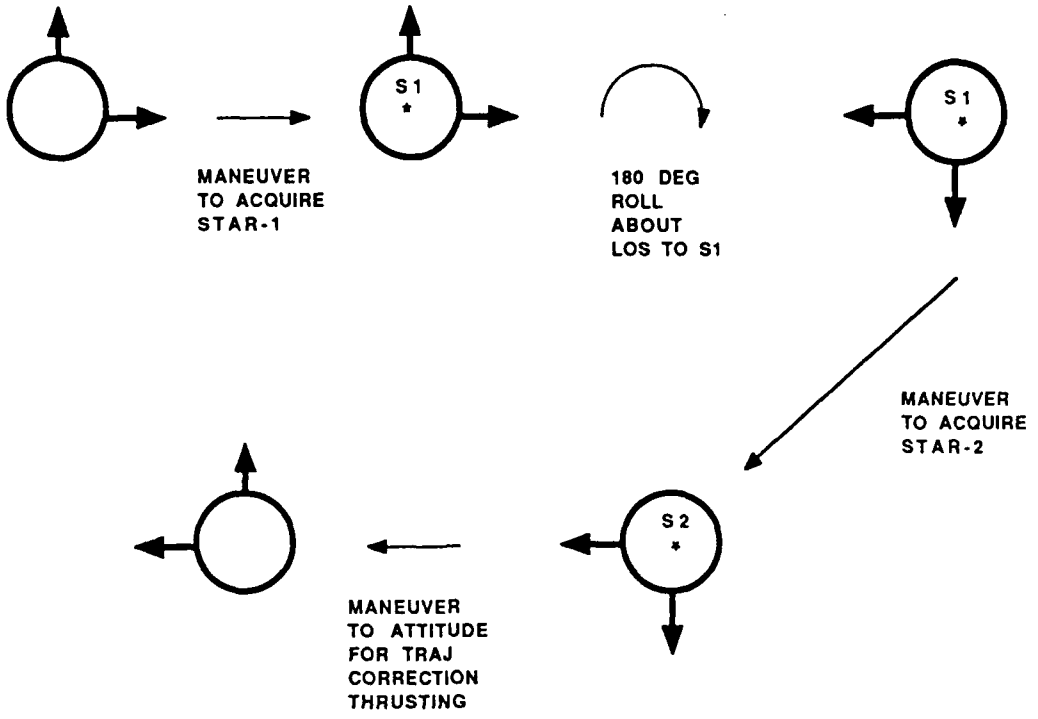

Fig. 3–2. Star Acquisition Maneuver and 180–Degree Roll about LOS to Star

only one star is sighted for update.

Figure 4–1 compares the navigation performance in terms of normalized CEP of the four system configurations for various mechanization options. It is shown that zero–g update is necessary for the pendulus accelerometer based strapdown system, i.e. SD/3A. Notice that the CEPs for the cases of no zero–g update are not plotted due to the excessive error magnitude. This is because the post boost zero–g update complements preflight one–g measurement for calibration observability of the roll axis accelerometer. A high performance accelerometer, e.g. SFIR, with good bias and scale factor stability aiding the strapdown IMU triad, i.e. the SD/4A configuration, allows medium accuracy performance for applications where zero–g update can not be performed. The single turn axis in the 1X/3A configuration enables the calibration of the bias and scale factor of the thrust axis accelerometer without the zero–g update. With the degrees of freedom provided by a two–axis gimbal, i.e. the 2X/3A configuration, complete IMU calibration can be accomplished preflight. Figure 4–1 also shows the benefits of the 180–degree roll about the LOS to the star. The difference between calibrating the star sensor LOS to IMU alignment using case fixed simulated star preflight and using the actual star post boost is minimum in terms of the CEP performance as indicated in comparing options A and B for the two–axis gimbaled configuration. The benefit of two–star update is not apparent in the Figure 4–1 comparison of options 2 and 3. This is because a star at target zenith is used in the case of one–star update offering near optimal performance. The real advantage of the two–star update lies in the lifting of constraints on star location. Any pair of bright and isolated star with adequate angular separation can be used to provide complete three axes attitude information. This relaxes the star sensor design requirement in that better signal to noise ratio can be assured.

Benefits of the single turn axis and the 180–degree roll about star LOS are not fully revealed in Figure 4–1 because of the good (and realistic) accelerometer bias and scale factor performance, and the alignment stability considered. Figure 4–2 compares the performance sensitivities to parameter variations for the four system configurations. Without zero–g update, the performance of the pure strapdown system, i.e. SD/4A, will be severely degraded in the presence of large shifts in the high accuracy aiding accelerometer bias and scale factor. A factor of ten degradation from nominal budget value is considered in the analysis as designated by HAX10 in Figure 4–2. The bias and scale factor can be calibrated to the extent allowed by the IA misalignment using the single turn axis to point the IA up and down in the preflight environment. Full calibration is achieved through stellar update because of the correlation between the preflight alignment error and the IA misalignment. The performance sensitivity to the star sensor LOS to IMU misalignment is analyzed considering a factor of ten increase over the budget as designated by LOSX10 in Figure 4–2. This level of misalignment is excessive; however, it points out the possibility of flight test evaluation of the system concept by simply flying an AIMU piggy back onboard the missile with an existing star sensor. The benefit of the 180–degree roll is dramatic. With a two–axis gimbal, the roll about LOS can be accomplished using the inner gimbal rotation. Figure 4–2 shows this should be done unless the alignment stability is assured or a preflight calibration is performed rolling about the LOS to a case fixed simulated star.

Additional performance sensitivities to system parameter variations are presented in Figure 4–3. The performance for 50 % increases in zero–g noise and gyro angular random walk are designated as ZRG and ARW respectively. The effect of uncertainty in initial position, designated as PIC, represents 100 fold increases in north and east components of launch point uncertainty. The zero–g update noise determines the accelerometer calibration accuracy which translates directly to down range target miss. The gyro angular random walk degrades the correlation between the navigation and attitude errors and thus reduces the effectiveness of the stellar update which is basically an accurate attitude measurement. The horizontal components of launch point uncertainty produce preflight level alignment errors similar to horizontal components of accelerometer bias and IA misalignment. Zero–g update provides direct observation on accelerometer bias. The preflight level alignment error is observed by the star sightings leaving the effect of accelerometer IA misalignment and launch point uncertainty indistinguishable. This is not a problem for a silo based system since launch point is well surveyed. Nor is it a problem for a two axes gimbaled system because accelerometer bias and IA misalignment are fully calibrated

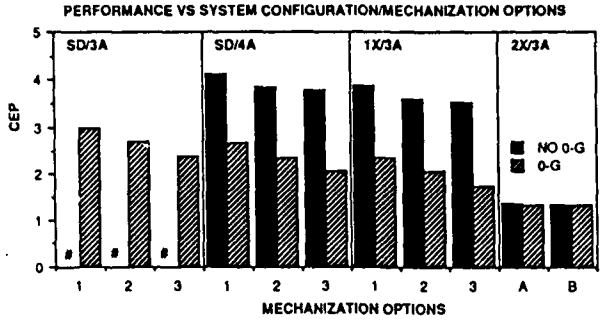

NOTES:

PLOTS FOR SD/3A-NO 0-G NOT SHOWN

OPTION	NO. OF STAR	LOS-ROLL
1	1	NO
2	1	YES
3	2	YES
A	2	YES (PREFLIGHT)
B	2	YES

Fig. 4–1. Comparison of CEP Performance for Various System Configurations and Mechanization Options

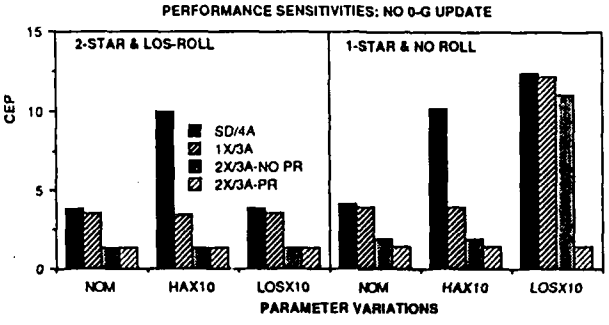

NOTES:

*PR: PREFLIGHT ROLL ABOUT LOS TO CASE FIXED SIMULATED STAR
*NO PR: NO PREFLIGHT ROLL
*NOM: NOMINAL ERROR BUDGET
*HAX10: 10 TIMES BUDGET HIGH ACCURACY ACCEL BIAS, SF AND IA MISALIGNMENT
*LOSX10: 10 TIMES BUDGET STAR SENSOR LOS MISALIGNMENT TO IMU

Fig. 4–2. Performance Sensitivities to Aiding Accelerometer Error and Star Sensor LOS to IMU Misalignment

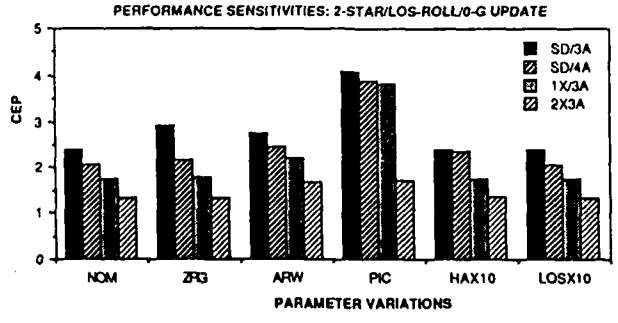

NOTES:

*SYSTEM OPERATIONS INCLUDE 2-STAR STELLAR AIDING, ROLL ABOUT LOS TO STAR AND POST BOOST ZERO-G UPDATE
*NOM: NOMINAL ERROR BUDGET
*ZRG: 50 % INCREASE OF ZERO-G UPDATE ERROR
*ARW: 50 % INCREASE OF GYRO ANGULAR RANDOM WALK
*PIC: FACTOR OF 100 INCREASE OF INITIAL NORTH AND EAST POSITION UNCERTAINTY
*HAX10: 10 TIMES BUDGET HIGH ACCURACY ACCEL BIAS, SF AND IA MISALIGNMENT
*LOSX10: STAR SENSOR LOS MISALIGNMENT TO IMU 10 TIMES NOMINAL BUDGET VALUE

Fig. 4–3. Performance Sensitivity to Parameter Variations

preflight. The two–axis gimbaled system may be required for a mobile missile system because of the IA stability capability of the pendulus accelerometer.

The top fifteen error sources for the SD/4A configuration are presented in Figure 4–4 for the case of a full complement of inflight update operations. The CEP is used as a scalar figure of merit in the ranking of the significance of error sources. As expected the top error source is the gyro angular random walk because of its degrading correlation effects. This is followed by the zero–g update noise and the velocity noise during preflight C & A because of their influence on the accelerometer calibration. Almost equally significant are the aiding accelerometer scale factor and bias errors. The accelerometer IA misalignments are contributing to the target miss but at lesser significance.

The same system aided with sighting to a single star is analyzed with the top fifteen error sources identified in Figure 4–5. The over all system performance is degraded by a factor of two. However, this represents a greatly relaxed requirement on vehicle capability. It can be implemented near the end of the third stage rocket propulsion prior to thrust termination. Without a zero–g update for the accelerometer bias determination, and lacking the complete three–axis attitude information, accelerometer bias and IA misalignments become dominant. The inability to calibrate the thrust axis accelerometer scale factor increases the significance of this error source. The lack of 180–degree roll about star LOS also increases the contribution to target miss by the star sensor to IMU misalignment.

The top fifteen error sources for the 1X/3A configuration are presented in Figure 4–6 for the case of a full complement of inflight updates. The gyro angular random walk again is the top error source. The ability to calibrate the aiding accelerometer scale factor preflight reduces the significance of zero–g update noise only slightly. This is so because resolution of pitch and yaw axis accelerometer bias and accelerometer IA misalignment are still dependent on zero–g update. The same system aided with sighting to a single star is analyzed with the ranking of the top fifteen errors presented in Figure 4–7. The ordering of the error sources is quite similar to that presented in Figure 4–5.

The top fifteen error sources for the 2X/3A configuration are presented in Figure 4–8 for the case of a full complement of inflight updates. This represents the best performing system. The gyro angular random walk and velocity noise during preflight calibration and alignment are the top error sources.

5. Technology Status

The key elements of a stellar aided RLG IMU include the RLGs, the accelerometers and the star sensor. Recent developments in these key technology areas include the development by BMO of a RLG based strapdown Advanced IMU (AIMU) for application to strategic weapon systems and the demonstration of a stellar aided stable platform IMU as part of the Alternate Inertial Navigation System (AINS) on Air Force's SICBM program. High performance accelerometers such as SFIR are already in production for existing missile systems with proven performance and radiation hardness. The development of a high performance Vibrating Beam Accelerometer (VBA), also under BMO sponsorship is in progress aiming toward lower cost, higher reliability and improved size, power and weight characteristics.

5.1 RLG/Strapdown Technology–AIMU. The AIMU is a second generation development to the Dormant Inertial Navigation System (DINS) which was successfully flown aboard the Advanced Maneuvering Reentry Missile (AMaRV) and more recently on the Antenna Test Vehicle (ATV). AIMU is intended for application to maneuvering reentry vehicle guidance, e.g. Evader MaRV, Earth Penetrator Weapon (EPW) etc.. Honeywell's AIMU is a strapdown IMU consisting of three GG1320 ring laser gyros and three Bell XI–82 pendulus accelerometers mounted in an Inertial Sensor Assembly

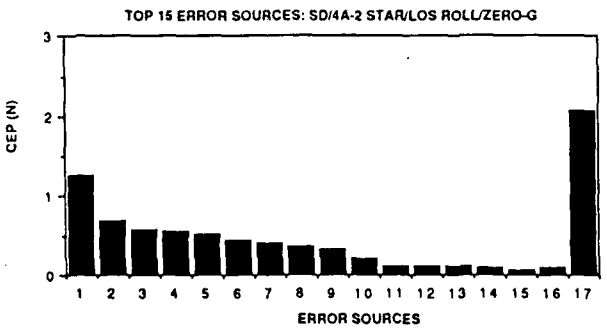

INFLIGHT UPDATES:
2-STAR STELLAR AIDING, 180-DEG ROLL ABOUT LOS TO STAR, ZERO-G UPDATE

TOP 15 ERROR SOURCES:

1 GYRO ANGULAR RANDOM WALK	2 ZERO-G NOISE
3 PREFLIGHT VELOCITY NOISE	4 ACCEL SF (AIDING A4-HA)
5 GYRO IA MISALIGN (G2 ABOUT 1)	6 ACCEL IA MISALIGN (A3 ABOUT 2)
7 ACCEL BIAS (AIDING A4-HA)	8 GYRO BIAS (G1)
9 STAR SENSOR NOISE	10 ACCEL IA MISALIGN (A2 ABOUT 3)
11 ACCEL IA MISALIGN (A1 ABOUT 2)	12 GYRO SF (G3)
13 ACCEL IA MISALIGN (A2 ABOUT 1)	14 GYRO BIAS (G3)
15 GYRO IA MISALIGN (G1 ABOUT 2)	16 ALL OTHER ERRORS
17 ALL ERROR SOURCES	

Fig. 4–4. Top Fifteen Error Sources for SD/4A System Configuration With Full Complement of Post Boost Aiding Operations

(ISA), inertial sensor electronics, a system clock, an inertial data processor, and a navigation processor and associated software. A specific objective of the AIMU program is to develop and qualify the radiation hard ISA for full scale production. Contracts were awarded to Honeywell and Rockwell in September 1987 for development of this system. The program recently completed a successful preliminary design review. AIMU engineering test unit fabrication and assembly is in full swing with scheduled delivery in July 1989 for the ground test program evaluation including laboratory, centrifuge, and sled testing.

5.2 Stellar Technology Demonstrated Application. Stellar technology is a mature concept having been reliably deployed in boost guidance applications on both Navy Trident I and II programs. The stellar subsystem developed by GE during the Air Force's recent Small Missile program was proven to meet all requirements as demonstrated in component, sled, and MM III flight tests. The heart of the GE/AINS stellar subsystem is a telescope with a Charge Injection Device (CID). The CID is a MOS imaging array of adjacent photo sensitive sites called pixels that are sensitive to photons in the 400 to 1000 nanometer range. On-chip electronics permit reading the photon-generated charge in each site. The CID's behavior in radiation allows the sighting to occur despite nuclear events.

Overall performance of this system was successfully demonstrated in sled tests and two MM III piggyback flight tests. In addition, the CID was proven to meet all specified hostile environments by component testing.

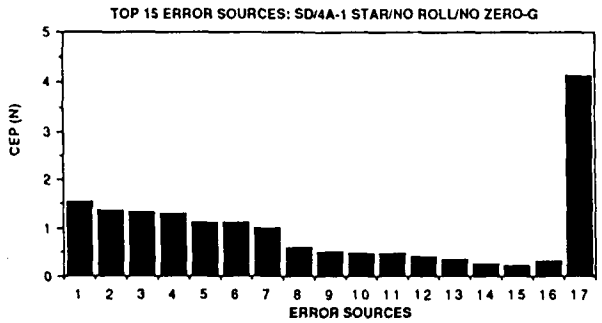

INFLIGHT UPDATES:
1-STAR STELLAR AIDING, NO ROLL ABOUT LOS TO STAR, NO ZERO-G UPDATE

TOP 15 ERROR SOURCES:

1 ACCEL BIAS (A3)	2 ACCEL IA MISALIGN (A2 ABOUT 3)
3 ACCEL IA MISALIGN (A3 ABOUT 2)	4 ACCEL BIAS (A2)
5 ACCEL SF (AIDING A4-HA)	6 STAR SENSOR LOS (#2)
7 GYRO ANGULAR RANDOM WALK	8 STAR SENSOR LOS (#3)
9 STAR SENSOR NOISE	10 ACCEL BIAS (AIDING A4-HA)
11 GYRO IA MISALIGN (G2 ABOUT 1)	12 PREFLIGHT VELOCITY NOISE
13 GYRO IA MISALIGN (G1 ABOUT 2)	14 ACCEL IA MISALIGN (A1 ABOUT 2)
15 ACCEL IA MISALIGN (A2 ABOUT 1)	16 ALL OTHER ERRORS
17 ALL ERROR SOURCES	

Fig 4-5. Top Fifteen Error Sources for SD/4A System Configuration Aiding With Sighting to a Single Star

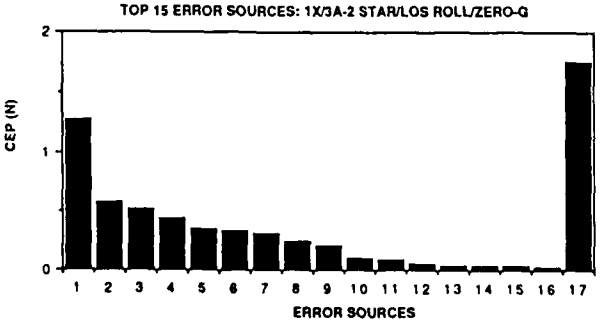

INFLIGHT UPDATES:
2-STAR STELLAR AIDING, 180-ROLL ABOUT LOS TO STAR, ZERO-G UPDATE

TOP 15 ERROR SOURCES:

1 GYRO ANGULAR RANDOM WALK	2 PREFLIGHT VELOCITY NOISE
3 GYRO IA MISALIGN (G2 ABOUT 1)	4 ACCEL IA MISALIGN (A3 ABOUT 2)
5 GYRO BIAS (G1)	6 STAR SENSOR NOISE
7 ZERO-G NOISE	8 ACCEL IA MISALIGN (A2 ABOUT 1)
9 ACCEL IA MISALIGN (A2 ABOUT 3)	10 GYRO SCALE FACTOR (G3)
11 GYRO BIAS (G3)	12 GYRO IA MISALIGN (G1 ABOUT 2)
13 GYRO BIAS (G2)	14 ACCEL IA MISALIGN (A1 ABOUT 3)
15 ACCEL BIAS (A1-HA)	16 ALL OTHER ERRORS
17 ALL ERROR SOURCES	

Fig. 4-6. Top Fifteen Error Sources for IX/3A System Configuration With Full Complement of Post Boost Aiding Operations

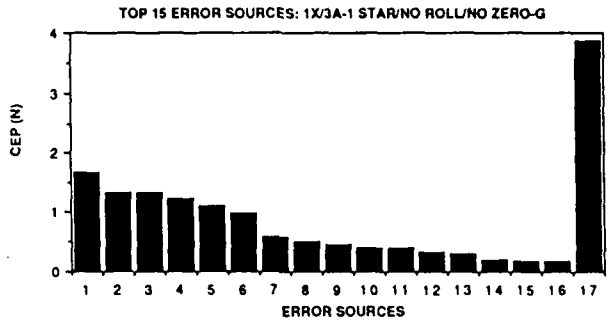

INFLIGHT UPDATES:
1-STAR STELLAR AIDING, NO ROLL ABOUT LOS TO STAR, NO ZERO-G UPDATE

TOP 15 ERROR SOURCES:

1 ACCEL BIAS (A3)	2 ACCEL IA MISALIGN (A2 ABOUT 3)
3 ACCEL IA MISALIGN (A3 ABOUT 2)	4 ACCEL BIAS (A2)
5 STAR SENSOR LOS (#2)	6 GYRO ANGULAR RANDOM WALK
7 STAR SENSOR LOS (#3)	8 STAR SENSOR NOISE
9 GYRO IA MISALIGN (G2 ABOUT 1)	10 ACCEL SF (A1-HA)
11 PREFLIGHT VELOCITY NOISE	12 GYRO IA MISALIGN (G1 ABOUT 2)
13 ACCEL IA MISALIGN (A2 ABOUT 1)	14 GYRO BIAS (G1)
15 ACCEL BIAS (A1-HA)	16 ALL OTHER ERRORS
17 ALL ERROR SOURCES	

Fig 4–7. Top Fifteen Error Sources for IX/3A System Configuration Aiding With Sighting to a Single Star

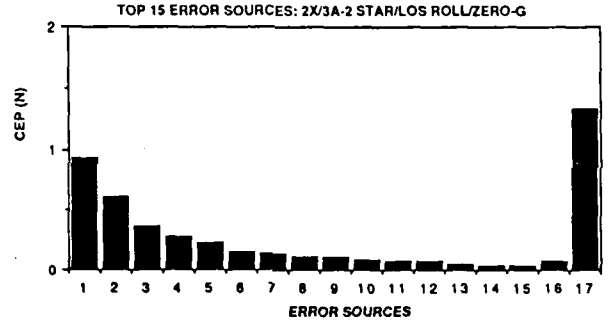

INFLIGHT UPDATES:
2-STAR STELLAR AIDING, 180-DEG ROLL ABOUT LOS TO STAR, ZERO-G UPDATE

TOP 15 ERROR SOURCES:

1 GYRO ANGULAR RANDOM WALK	2 PREFLIGHT VELOCITY NOISE
3 STAR SENSOR NOISE	4 GYRO IA MISALIGN (G2 ABOUT 1)
5 GYRO IA MISALIGN (G1 ABOUT 2)	6 ZERO-G NOISE
7 ACCEL SF (A1-HA)	8 GYRO IA MISALIGN (G3 ABOUT 2)
9 GYRO IA MISALIGN (G1 ABOUT 3)	10 ACCEL BIAS (A1-HA)
11 GYRO IA MISALIGN (G2 ABOUT 3)	12 ACCEL IA MISALIGN (A1 ABOUT 3)
13 ACCEL IA MISALIGN (A3 ABOUT 1)	14 GYRO BIAS (G3)
15 GYRO BIAS (G2)	16 ALL OTHER ERRORS
17 ALL ERROR SOURCES	

Fig. 4–8. Top Fifteen Error Sources for 2X/3A System Configuration With Full Complement of Post Boost Aiding Operations

6. Conclusions

Stellar aided RLG IMUs offer high accuracy missile guidance performance. The stellar aiding relaxes the requirement of preflight azimuth alignment eliminating the need of expensive high performance gyros. The use of a semi–dormant system with a stellar sensor and the laser gyros is the primary driver for lower cost and high reliability. This is possible because of the cost and reliability benefits directly associated with RLG and the simplification in star sensor design enabled by the excellent scale factor performance of the RLG. Use of single turn axis offers a cost effective solution to preflight calibration of the thrust axis accelerometer scale factor. The two axis gimbaled system offers complete field calibration capability to deliver performance comparable to the best existing ICBM guidance IMUs at potentially significantly lowered cost and enhanced reliability.